Journal of Computational Mathematics, Vol.27, No.5, 2009, 573–603.

Local Multigrid in H(curl)*

Ralf Hiptmair
SAM, ETH Zürich, CH-8092 Zürich, Switzerland
Email: hiptmair@sam.math.ethz.ch
Weiying Zheng
LSEC, ICMSEC, Academy of Mathematics and System Sciences, Chinese Academy of Sciences, Beijing 100190, China
Email: zwy@lsec.cc.ac.cn

Abstract

We consider $\boldsymbol{H}(\mathbf{curl},\Omega)$-elliptic variational problems on bounded Lipschitz polyhedra and their finite element Galerkin discretization by means of lowest order edge elements. We assume that the underlying tetrahedral mesh has been created by successive local mesh refinement, either by local uniform refinement with hanging nodes or bisection refinement. In this setting we develop a convergence theory for the the so-called local multigrid correction scheme with hybrid smoothing. We establish that its convergence rate is uniform with respect to the number of refinement steps. The proof relies on corresponding results for local multigrid in a $H^1(\Omega)$-context along with local discrete Helmholtz-type decompositions of the edge element space.

Mathematics subject classification: 65N30, 65N55, 78A25.
Key words: Edge elements, Local multigrid, Stable multilevel splittings, Subspace correction theory, Regular decompositions of $\boldsymbol{H}(\mathbf{curl},\Omega)$, Helmholtz-type decompositions, Local mesh refinement.

1. Introduction

On a polyhedron $\Omega\subset\mathbb{R}^3$, scaled such that $\operatorname{diam}(\Omega)=1$, we consider the variational problem: seek $\mathbf{u}\in\boldsymbol{H}_{\Gamma_D}(\mathbf{curl},\Omega)$ such that

$$\underbrace{(\mathbf{curl}\,\mathbf{u},\mathbf{curl}\,\mathbf{v})_{L^2(\Omega)}+(\mathbf{u},\mathbf{v})_{L^2(\Omega)}}_{=:\mathsf{a}(\mathbf{u},\mathbf{v})}=(\mathbf{f},\mathbf{v})_{L^2(\Omega)}\quad\forall\mathbf{v}\in\boldsymbol{H}_{\Gamma_D}(\mathbf{curl},\Omega)\,. \tag{1.1}$$

For the Hilbert space of square integrable vector fields with square integrable **curl** and vanishing tangential components on Γ_D we use the symbol $\boldsymbol{H}_{\Gamma_D}(\mathbf{curl},\Omega)$, see [22, Ch. 1] for details. The source term $\mathbf{f}$ in (1.1) is a vector field in $(L^2(\Omega))^3$. The left hand side of (1.1) agrees with the inner product of $\boldsymbol{H}_{\Gamma_D}(\mathbf{curl},\Omega)$ and will be abbreviated by $\mathsf{a}(\mathbf{u},\mathbf{v})$ ("energy inner product").

Further, Γ_D denotes the part of the boundary $\partial\Omega$ on which homogeneous Dirichlet boundary conditions in the form of vanishing tangential traces of $\mathbf{u}$ are imposed. The geometry of the Dirichlet boundary part Γ_D is supposed to be simple in the following sense: for each connected component Γ_i of Γ_D we can find an open Lipschitz domain $\Omega_i\subset\mathbb{R}^3$ such that

$$\overline{\Omega}_i\cap\overline{\Omega}=\Gamma_i\,,\quad \Omega_i\cap\Omega=\emptyset\,, \tag{1.2}$$

* Received December 12, 2007 / Revised version received November 5, 2008 / Accepted February 5, 2009 /

Table 1.1: Important notation used in this paper

$\boldsymbol{H}(\mathbf{curl},\Omega)$	: Sobolev space of square integrable vector fields on $\Omega\subset\mathbb{R}^3$ with square integrable **curl**
$\boldsymbol{H}_{\Gamma_D}(\mathbf{curl},\Omega)$	: vector fields in $\boldsymbol{H}(\mathbf{curl},\Omega)$ with vanishing tangential components on $\Gamma_D\subset\partial\Omega$
$\mathcal{M}$, $\mathcal{T}$	: tetrahedral finite element meshes, may contain hanging nodes
$\mathcal{N}(\mathcal{M})$	: set of vertices (nodes) of a mesh $\mathcal{M}$
$\mathcal{E}(\mathcal{M})$	: set of edges of a mesh $\mathcal{M}$
$\rho_K,\rho_{\mathcal{M}}$	: shape regularity measures
h	: – local meshwidth function for a finite element mesh – (as subscript) tag for finite element functions
$\mathbf{U}(\mathcal{M})$	: lowest order edge element space on $\mathcal{M}$
$\mathbf{b}_E$	: nodal basis function of $\mathbf{U}(\mathcal{M})$ associated with edge E
$V(\mathcal{M})$	: space of continuous piecewise linear functions on $\mathcal{M}$
$V_2(\mathcal{M})$	: quadratic Lagrangian finite element space on $\mathcal{M}$
$\widetilde{V}_2(\mathcal{M})$	: quadratic surplus space, see (2.19)
$b_{\boldsymbol{p}}$	: nodal basis function of $V(\mathcal{M})$ ("tent function") associated with vertex $\boldsymbol{p}$
$\mathfrak{B}_X(\mathcal{M})$	: set of nodal basis functions for finite element space X on mesh $\mathcal{M}$
$\boldsymbol{\Pi}_h$	: nodal edge interpolation operator onto $\mathbf{U}(\mathcal{M})$, see (2.7)
$\mathcal{I}_h$	: vertex based piecewise linar interpolation onto $V(\mathcal{M})$
$\mathbb{P}_p$	: space of 3-variate polynomials of total degree $\le p$
$\overline{\mathbf{U}}(\mathcal{M})$, $\overline{V}(\mathcal{M})$	: finite element spaces oblivious of zero boundary conditions
$\prec$	: nesting of finite element meshes
$\ell(K)$	: level of element K in hierarchy of refined meshes
ω_l	: refinement zone, see (4.1)
Σ_l	: refinement strip, see (5.35)
$\mathfrak{B}_V^l$, $\mathfrak{B}_{\mathbf{U}}^l$	: sets of basis functions supported inside refinement zones, see (4.9)
Q_h	: quasi-interpolation operator for linear Lagrangian finite elements

and Ω_i and Ω_j have positive distance for $i\neq j$. Further, the interior of $\overline{\Omega}\cup\overline{\Omega_1}\cup\overline{\Omega_2}\ldots$ is expected to be a Lipschitz-domain, too (see Fig. 5.1). This is not a severe restriction, because variational problems related to (1.1) usually arise in quasi-static electromagnetic modelling, where simple geometries are common. Of course, $\Gamma_D=\emptyset$ is admitted.

Lowest order $\boldsymbol{H}_{\Gamma_D}(\mathbf{curl},\Omega)$-conforming edge elements are widely used for the finite element Galerkin discretization of variational problems like (1.1). Then, for a solution $\mathbf{u}\in(H^1(\Omega))^3$ with $\mathbf{curl}\,\mathbf{u}\in(H^1(\Omega))^3$ we can expect the optimal asymptotic convergence rate

$$\|\mathbf{u}-\mathbf{u}_h\|_{\boldsymbol{H}(\mathbf{curl},\Omega)}\le CN_h^{-1/3}\,, \tag{1.3}$$

on families of finite element meshes arising from global refinement. Here, $\mathbf{u}_h$ is the finite element solution, N_h the dimension of the finite element space, and $C>0$ does not depend on N_h. However, often $\mathbf{u}$ will fail to possess the required regularity due to singularities arising at edges/corners of $\partial\Omega$ and material interfaces [20, 21]. Fortunately, it seems to be possible to retain (1.3) by the use of adaptive local mesh refinement based on a posteriori error estimates, see [10, 47] for theory in H^1-setting, [7, 17] for numerical evidence in the case of edge element discretization, and [8, 31, 45] for related theoretical investigations.

We also need ways to *compute* the asymptotically optimal finite element solution with optimal computational effort, that is, with a number of operations proportional to N_h. This can only be achieved by means of iterative solvers, whose convergence remains fast regardless of the depth of refinement. Multigrid methods are the most prominent class of iterative solvers that achieve this goal. By now, geometric multigrid methods for discrete $\boldsymbol{H}(\mathbf{curl},\Omega)$-elliptic variational problems like (1.1) have become well established [19, 25, 46, 50]. Their asymptotic theory on sequencies of regularly refined meshes has also matured [2, 23, 25, 27, 44]. It confirms *asymptotic optimality*: the speed of convergence is uniformly fast regardless of the number of refinement levels involved. In addition, the costs of one step of the iteration scale linearly with the number of unknowns.

Yet, the latter property is lost when the standard multigrid correction scheme is applied to meshes generated by pronounced local refinement. Optimal computational costs can only be maintained, if one adopts the local multigrid policy, which was pioneered by A. Brandt et al. in [5], see also [36]. Crudely speaking, its gist is to confine relaxations to "new" degrees of freedom located in zones where refinement has changed the mesh. Thus an exponential increase of computational costs with the number of refinement levels can be avoided: the total costs of a V-cycle remain proportional to the number of unknowns. An algorithm blending the local multigrid idea with the geometric multigrid correction scheme of [25] is described in [46]. On the other hand, a proof of uniform asymptotic convergence has remained elusive so far. It is the objective of this paper to provide it, see Theorem 4.2.

We recall the key insight that (1.1) is one member of a family of variational problems. Its kin is obtained by replacing **curl** with **grad** or div, respectively. All these differential operators turn out to be incarnations of the fundamental exterior derivative of differential geometry, *cf.* [25, Sect. 2]. They are closely connected in the deRham complex [3] and, thus, it is hardly surprising that results about the related $H^1_{\Gamma_D}(\Omega)$-elliptic variational problem, which seeks $u \in H^1_{\Gamma_D}(\Omega)$ such that

$$(\mathbf{grad}u,\mathbf{grad}v)_{L^2(\Omega)} + (u,v)_{L^2(\Omega)} = (f,v)_{L^2(\Omega)} \quad \forall\, v \in H^1_{\Gamma_D}(\Omega)\;, \tag{1.4}$$

prove instrumental in the multigrid analysis for discretized versions of (1.1). Here $H^1_{\Gamma_D}(\Omega)$ is the subspace of $H^1(\Omega)$ whose functions have vanishing traces on Γ_D.

Thus, when tackling (1.1), we take the cue from the local multigrid theory for (1.4) discretized by means of linear continuous finite elements. This theory has been developed in various settings, *cf.* [5, 11, 14, 15, 54]. In [1] local refinement with hanging nodes is treated. Recently, Wu and Chen [52] proved the uniform convergence of local multigrid V-cycles on adaptively refined meshes in two dimensions. Their mesh refinements are controlled by a posteriori error estimators and carried out according to the "newest vertex bisection" strategy introduced, independently, in [6, 35].

As in the case of global multigrid, the essential new aspect of local multigrid theory for (1.1) compared to (1.4) is the need to deal with the kernel of the **curl**-operator, *cf.* [25, Sect. 3]. In this context, the availability of discrete scalar potential representations for irrotational edge element vector fields is pivotal. Therefore, we devote the entire Sect. 2 to the discussion of edge elements and their relationship with conventional Lagrangian finite elements. Meshes with hanging nodes will receive particular attention. Next, in Sect. 3 we present details about local mesh refinement, because some parts of the proofs rest on the subtleties of how elements are split. The following Sect. 4 introduces the local multigrid method from the abstract perspective of successive subspace correction.

The proof of uniform convergence (Theorem 4.2) is tackled in Sect. 5, which forms the core of the article. In particular, the investigation of the stability of the local multilevel splitting requires several steps. The foundation is provided by a well-known stability result for the bilinear form from (1.4) and linear finite elements. Another ingredient are continuous and discrete Helmholtz-type decompositions covered in Sect. 5.1. Many developments are rather technical and to aid the reader important notations are listed in Table 1.1. Eventually, in Sect. 6, we report two numerical experiments to show the competitive performance of the local multigrid method and the relevance of the convergence theory.

Remark 1.1. In this article we forgo generality and do not discuss the more general bi-linear form

$$\mathsf{a}(\mathbf{u},\mathbf{v}) := (\alpha\,\mathbf{curl}\,\mathbf{u},\mathbf{curl}\,\mathbf{v})_{L^2(\Omega)} + (\beta\mathbf{u},\mathbf{v})_{L^2(\Omega)}\ , \quad \forall \mathbf{u},\mathbf{v} \in \boldsymbol{H}_{\Gamma_D}(\mathbf{curl},\Omega)\ , \tag{1.5}$$

with uniformly positive coefficient functions $\alpha,\beta \in L^\infty(\Omega)$. We do this partly for the sake of lucidity and partly, because the current theory cannot provide estimates that are robust with respect to large variations of α and β, *cf.* [29]. We refer to [55] for further information and references.

2. Finite Element Spaces

Whenever we refer to a finite element mesh in this article, we have in mind a tetrahedral triangulation of Ω, see [18, Ch. 3]. In certain settings, it may feature hanging nodes, that is, the face of one tetrahedron can coincide with the union of faces of other tetrahedra. Further, the mesh is supposed to resolve the Dirichlet boundary in the sense that Γ_D is the union of faces of tetrahedra. The symbol $\mathcal{M}$ with optional subscripts is reserved for finite element meshes and the sets of their elements alike.

We write $h \in L^\infty(\Omega)$ for the piecewise constant function, which assumes value $h_K := \operatorname{diam}(K)$ in each element $K \in \mathcal{M}$. The ratio of $\operatorname{diam}(K)$ to the radius of the largest ball contained in K is called the shape regularity measure ρ_K [18, Ch. 3, §3.1]. The shape regularity measure $\rho_{\mathcal{M}}$ of $\mathcal{M}$ is the maximum of all ρ_K, $K \in \mathcal{M}$.

2.1. Conforming meshes

Provisionally, we consider only finite element meshes $\mathcal{M}$ that are conforming, that is, each face of a tetrahedron is either contained in $\partial\Omega$ or a face of another tetrahedron, see [18, Ch. 2, § 2.2]. In particular, this rules out hanging nodes. Following [12, 38], we introduce the space of lowest order $\boldsymbol{H}_{\Gamma_D}(\mathbf{curl},\Omega)$-conforming edge finite elements, also known as Whitney-1-forms [51],

$$\mathbf{U}(\mathcal{M}) := \{\mathbf{v}_h \in \boldsymbol{H}_{\Gamma_D}(\mathbf{curl},\Omega) :\ \forall K \in \mathcal{M} : \exists\, \boldsymbol{a},\boldsymbol{b} \in \mathbb{R}^3 : \tag{2.1}$$

$$\mathbf{v}_h(\boldsymbol{x}) = \boldsymbol{a} + \boldsymbol{b} \times \boldsymbol{x},\ \boldsymbol{x} \in K\}\ . \tag{2.2}$$

For a detailed derivation and description please consult [26, Sect. 3] or the monographs [13, 37]. Notice that $\mathbf{curl}\,\mathbf{U}(\mathcal{M})$ is a space of piecewise constant vector fields. We also remark that appropriate global degrees of freedom (d.o.f.) for $\mathbf{U}(\mathcal{M})$ are given by

$$\left\{ \begin{array}{rcl} \mathbf{U}(\mathcal{M}) & \mapsto & \mathbb{R} \\ \mathbf{v}_h & \mapsto & \int_E \mathbf{v}_h \cdot \mathrm{d}\vec{s} \end{array} \right. , \quad E \in \mathcal{E}(\mathcal{M})\ , \tag{2.3}$$

where $\mathcal{E}(\mathcal{M})$ is the set of edges of $\mathcal{M}$ not contained in Γ_D. We write $\mathfrak{B}_{\mathbf{U}}(\mathcal{M})$ for the nodal basis of $\mathbf{U}(\mathcal{M})$ dual to the global d.o.f. (2.3). Basis functions are associated with active edges. Hence, we can write $\mathfrak{B}_{\mathbf{U}}(\mathcal{M}) = \{\mathbf{b}_E\}_{E\in\mathcal{E}(\mathcal{M})}$. The support of the basis function $\mathbf{b}_E$ is the union of tetrahedra sharing the edge E. We recall the simple formula for local shape functions

$$\mathbf{b}_{E|K} = \lambda_i \mathbf{grad}\lambda_j - \lambda_j \mathbf{grad}\lambda_i \quad E = [\boldsymbol{a}_i, \boldsymbol{a}_j] \subset \overline{K} \tag{2.4}$$

for any tetrahedron $K \in \mathcal{M}$ with vertices $\boldsymbol{a}_i$, $i = 1, 2, 3, 4$, and associated barycentric coordinate functions λ_i.

The edge element space $\mathbf{U}(\mathcal{M})$ with basis $\mathfrak{B}_{\mathbf{U}}(\mathcal{M})$ is perfectly suited for the finite element Galerkin discretization of (1.1). The discrete problem based on $\mathbf{U}(\mathcal{M})$ reads: seek $\mathbf{u}_h \in \mathbf{U}(\mathcal{M})$ such that

$$(\mathbf{curl}\,\mathbf{u}_h, \mathbf{curl}\,\mathbf{v}_h)_{L^2(\Omega)} + (\mathbf{u}_h, \mathbf{v}_h)_{L^2(\Omega)} = (\mathbf{f}, \mathbf{v}_h)_{L^2(\Omega)} \quad \forall \mathbf{v}_h \in \mathbf{U}(\mathcal{M}) \,. \tag{2.5}$$

The properties of $\mathbf{U}(\mathcal{M})$ will be key to constructing and analyzing the local multigrid method for the large sparse linear system of equations resulting from (2.5). Next, we collect important facts.

The basis $\mathfrak{B}_{\mathbf{U}}(\mathcal{M})$ enjoys uniform L^2-stability, meaning the existence of a constant[1)] $C = C(\rho_{\mathcal{M}}) > 0$ such that for all $\mathbf{v}_h = \sum\limits_{E\in\mathcal{E}(\mathcal{M})} \alpha_E \mathbf{b}_E \in \mathbf{U}(\mathcal{M})$, $\alpha_E \in \mathbb{R}$,

$$C^{-1} \|\mathbf{v}_h\|^2_{L^2(\Omega)} \leq \sum_{E\in\mathcal{E}(\mathcal{M})} \alpha_E^2 \|\mathbf{b}_E\|^2_{L^2(\Omega)} \leq C \|\mathbf{v}_h\|^2_{L^2(\Omega)} \,. \tag{2.6}$$

The global d.o.f. induce a nodal edge interpolation operator

$$\boldsymbol{\Pi}_h : \begin{cases} \mathrm{dom}(\boldsymbol{\Pi}_h) \subset \boldsymbol{H}_{\Gamma_D}(\mathbf{curl}, \Omega) & \mapsto \quad \mathbf{U}(\mathcal{M}) \\ \mathbf{v} & \mapsto \quad \sum\limits_{E\in\mathcal{E}(\mathcal{M})} \left(\int_E \mathbf{v}\cdot \mathrm{d}\vec{s}\right) \cdot \mathbf{b}_E \,. \end{cases} \tag{2.7}$$

Obviously, $\boldsymbol{\Pi}_h$ provides a local projection, but it turns out to be unbounded even on $(H^1(\Omega))^3$. Only for vector fields with discrete rotation the following interpolation error estimate is available, see [26, Lemma 4.6]:

Lemma 2.1. *The interpolation operator* $\boldsymbol{\Pi}_h$ *is bounded on* $\{\boldsymbol{\Psi} \in (H^1(\Omega))^3, \mathbf{curl}\,\boldsymbol{\Psi} \in \mathbf{curl}\,\mathbf{U}(\mathcal{M})\} \subset (H^1(\Omega))^3$, *and for any* conforming *mesh there is* $C = C(\rho_{\mathcal{M}}) > 0$ *such that*

$$\left\|h^{-1}(Id - \boldsymbol{\Pi}_h)\boldsymbol{\Psi}\right\|_{L^2(\Omega)} \leq C|\boldsymbol{\Psi}|_{H^1(\Omega)} \quad \forall \boldsymbol{\Psi} \in (H^1(\Omega))^3,\ \mathbf{curl}\,\boldsymbol{\Psi} \in \mathbf{curl}\,\mathbf{U}(\mathcal{M}) \,.$$

If Ω is homeomorphic to a ball, then

$$\mathbf{grad}H^1(\Omega) = \boldsymbol{H}(\mathbf{curl}\,0, \Omega) := \{\mathbf{v} \in \boldsymbol{H}(\mathbf{curl}, \Omega),\ \mathbf{curl}\,\mathbf{v} = 0\},$$

that is, $H^1(\Omega)$ provides scalar potentials for $\boldsymbol{H}(\mathbf{curl}, \Omega)$. To state a discrete analogue of this relationship we need the Lagrangian finite element space of piecewise linear continuous functions on $\mathcal{M}$

$$V(\mathcal{M}) := \{u_h \in H^1_{\Gamma_D}(\Omega) :\ u_{h|K} \in \mathbb{P}_1(K)\ \forall K \in \mathcal{M}\} \,, \tag{2.8}$$

[1)] The symbol C will stand for generic positive constants throughout this article. Its value may vary between different occurrences. We will always specify on which quantities these constants may depend.

where $\mathbb{P}_p(K)$ is the space of 3-variate polynomials of degree $\leq p$ on K. The global degrees of freedom for $V(\mathcal{M})$ boil down to point evaluations at the vertices of $\mathcal{M}$ away from $\overline{\Gamma}_D$ (set $\mathcal{N}(\mathcal{M})$). The dual basis of "tent functions" will be denoted by $\mathfrak{B}_V(\mathcal{M}) = \{b_{\boldsymbol{p}}\}_{\boldsymbol{p}\in\mathcal{N}(\mathcal{M})}$. Its unconditional L^2-stability is well known: with a universal constant $C > 0$ we have for all $u_h = \sum_{\boldsymbol{p}\in\mathcal{N}(\mathcal{M})} \alpha_{\boldsymbol{p}} b_{\boldsymbol{p}} \in V(\mathcal{M})$, $\alpha_{\boldsymbol{p}} \in \mathbb{R}$,

$$C^{-1} \|u_h\|^2_{L^2(\Omega)} \leq \sum_{\boldsymbol{p}\in\mathcal{N}(\mathcal{M})} \alpha^2_{\boldsymbol{p}} \|b_{\boldsymbol{p}}\|^2_{L^2(\Omega)} \leq C \|u_h\|^2_{L^2(\Omega)} \ . \tag{2.9}$$

For the nodal interpolation operator related to $\mathfrak{B}_V$ we write $\mathcal{I}_h : \mathrm{dom}(\mathcal{I}_h) \subset H^1_{\Gamma_D}(\Omega) \mapsto V(\mathcal{M})$. Recall the standard estimate for linear interpolation on *conforming* meshes (i.e., no hanging nodes allowed), [18, Thm. 3.2.1], that asserts the existence of $C = C(k, \rho_{\mathcal{M}}) > 0$ such that

$$\left\| h^{k-2}(Id - \mathcal{I}_h)u \right\|_{H^k(\Omega)} \leq C|u|_{H^2(\Omega)} \quad \forall u \in H^2(\Omega) \cap H^1_{\Gamma_D}(\Omega),\ k \in \{0, 1\} \ . \tag{2.10}$$

Obviously, $\mathbf{grad} V(\mathcal{M}) \subset \mathbf{U}(\mathcal{M})$, and immediate from Stokes theorem is the crucial *commuting diagram property*

$$\boldsymbol{\Pi}_h \circ \mathbf{grad} = \mathbf{grad} \circ \mathcal{I}_h \quad \text{on } \mathrm{dom}(\mathcal{I}_h) \ . \tag{2.11}$$

This enables us to give an elementary proof of Lemma 2.1.

Proof. [of Lemma 2.1] Pick one $K \in \mathcal{M}$ and, without loss of generality, assume $0 \in K$. Then define the lifting operator, *cf.* the "Koszul lifting" [3, Sect. 3.2],

$$\mathbf{w} \mapsto \mathcal{L}\,\mathbf{w} \ , \quad \mathcal{L}\,\mathbf{w}(\boldsymbol{x}) := \tfrac{1}{3}\mathbf{w}(\boldsymbol{x}) \times \boldsymbol{x} \ , \quad \boldsymbol{x} \in K \ . \tag{2.12}$$

Elementary calculations reveal that for any constant vectorfield $\mathbf{w} \in (\mathcal{P}_0(K))^3$

$$\mathbf{curl}\,\mathcal{L}\,\mathbf{w} = \mathbf{w} \ , \tag{2.13}$$

$$\|\mathcal{L}\,\mathbf{w}\|_{L^2(K)} \leq h_K \|\mathbf{w}\|_{L^2(K)} \ , \tag{2.14}$$

$$\mathcal{L}\,\mathbf{w} \in \mathbf{U}(K) \ . \tag{2.15}$$

The continuity (2.14) permits us to extend $\mathcal{L}$ to $(L^2(K))^3$.

Given $\boldsymbol{\Psi} \in (H^1(K))^3$ with $\mathbf{curl}\,\boldsymbol{\Psi} \equiv \mathrm{const}^3$, by (2.15) we know $\mathcal{L}\,\mathbf{curl}\,\boldsymbol{\Psi} \in (\mathcal{P}_1(K))^3$. Thus, an inverse inequality leads to

$$|\mathcal{L}\,\mathbf{curl}\,\boldsymbol{\Psi}|_{H^1(K)} \leq C h_K^{-1} \|\mathcal{L}\,\mathbf{curl}\,\boldsymbol{\Psi}\|_{L^2(K)} \overset{(2.14)}{\leq} C \|\mathbf{curl}\,\boldsymbol{\Psi}\|_{L^2(K)} \ , \tag{2.16}$$

with $C = C(\rho_K) > 0$. Next, (2.13) implies

$$\mathbf{curl}(\boldsymbol{\Psi} - \mathcal{L}\,\mathbf{curl}\,\boldsymbol{\Psi}) = 0 \quad \Rightarrow \quad \exists p \in H^1(K) : \quad \boldsymbol{\Psi} - \mathcal{L}\,\mathbf{curl}\,\boldsymbol{\Psi} = \mathbf{grad} p \ . \tag{2.17}$$

From (2.16) we conclude that $p \in H^2(K)$ and $|p|_{H^2(K)} \leq C|\boldsymbol{\Psi}|_{H^1(K)}$. Moreover, thanks to the commuting diagram property we have

$$\boldsymbol{\Psi} - \boldsymbol{\Pi}_h \boldsymbol{\Psi} = \underbrace{\mathcal{L}\,\mathbf{curl}\,\boldsymbol{\Psi} - \boldsymbol{\Pi}_h\,\mathcal{L}\,\mathbf{curl}\,\boldsymbol{\Psi}}_{=0 \text{ by } (2.15)} + \mathbf{grad}(p - \mathcal{I}_h p) \ , \tag{2.18}$$

which means, by the standard estimate (2.10) for linear interpolation on K,

$$\|\boldsymbol{\Psi} - \boldsymbol{\Pi}_h \boldsymbol{\Psi}\|_{L^2(K)} = |p - \mathcal{I}_h p|_{H^1(K)} \leq C h_K |p|_{H^2(K)} \leq C h_K |\boldsymbol{\Psi}|_{H^1(K)} \ .$$

Summation over all elements finishes the proof. □

As theoretical tools we need "higher order" counterparts of the above finite element spaces. We recall the quadratic Lagrangian finite element space

$$V_2(\mathcal{M}) := \{u_h \in H^1_{\Gamma_D}(\Omega) : \ u_{h|K} \in \mathbb{P}_2(K) \ \forall K \in \mathcal{M}\} \ , \tag{2.19}$$

and its subspace of quadratic surpluses

$$\widetilde{V}_2(\mathcal{M}) := \{u_h \in V_2(\mathcal{M}) : \ \mathcal{I}_h u_h = 0\} \ . \tag{2.20}$$

This implies a direct splitting

$$V_2(\mathcal{M}) = V(\mathcal{M}) \oplus \widetilde{V}_2(\mathcal{M}) \ , \tag{2.21}$$

which is unconditionally H^1-stable: there is a $C = C(\rho_{\mathcal{M}}) > 0$ such that

$$C^{-1}|u_h|^2_{H^1(\Omega)} \le |(Id - \mathcal{I}_h)u_h|^2_{H^1(\Omega)} + |\mathcal{I}_h u_h|^2_{H^1(\Omega)} \le C|u_h|^2_{H^1(\Omega)} \ , \tag{2.22}$$

for all $u_h \in V_2(\mathcal{M})$.

Next, we examine the space $(V(\mathcal{M}))^3$ of continuous piecewise linear vector fields that vanish on Γ_D. Standard affine equivalence techniques for edge elements, see [26, Sect. 3.6], confirm

$$\exists C = C(\rho_{\mathcal{M}}) > 0 : \quad \|\mathbf{\Pi}_h \mathbf{\Psi}_h\|_{L^2(\Omega)} \le C \, \|\mathbf{\Psi}_h\|_{L^2(\Omega)} \quad \forall \mathbf{\Psi}_h \in (V(\mathcal{M}))^3 \ . \tag{2.23}$$

Lemma 2.2. *For all $\mathbf{\Psi}_h \in (V(\mathcal{M}))^3$ we can find $\widetilde{v}_h \in \widetilde{V}_2(\mathcal{M})$ such that*

$$\mathbf{\Psi}_h = \mathbf{\Pi}_h \mathbf{\Psi}_h + \mathbf{grad}\widetilde{v}_h \ ,$$

and, with $C = C(\rho_{\mathcal{M}}) > 0$,

$$C^{-1} \, \|\mathbf{\Psi}_h\|^2_{L^2(\Omega)} \le \|\mathbf{\Pi}_h \mathbf{\Psi}_h\|^2_{L^2(\Omega)} + \|\mathbf{grad}\widetilde{v}_h\|^2_{L^2(\Omega)} \le C \, \|\mathbf{\Psi}_h\|^2_{L^2(\Omega)} \ .$$

For the proof we rely on a very useful insight, which relieves us from all worries concerning the topology of Ω:

Lemma 2.3. *If $\mathbf{v} \in \boldsymbol{H}_{\Gamma_D}(\mathbf{curl}\, 0, \Omega)$ and $\mathbf{\Pi}_h \mathbf{v} = 0$, then $\mathbf{v} \in \mathbf{grad} H^1_{\Gamma_D}(\Omega)$.*

Proof. Since the mesh covers Ω, the relative homology group $H_1(\Omega; \Gamma_D)$ is generated by a set of edge paths. By definition (2.3) of the d.o.f. of $\mathbf{U}(\mathcal{M})$, the path integrals of $\mathbf{v}$ along all these paths vanish. As an irrotational vector field with vanishing circulation along a complete set of Γ_D-relative fundamental cycles, $\mathbf{v}$ must be a gradient. □

Proof [of Lemma 2.2]. Given $\mathbf{\Psi}_h \in (V(\mathcal{M}))^3$, we decompose it according to

$$\mathbf{\Psi}_h = \mathbf{\Pi}_h \mathbf{\Psi}_h + \underbrace{(Id - \mathbf{\Pi}_h)\mathbf{\Psi}_h}_{=:\mathbf{grad}\widetilde{v}_h} \ . \tag{2.24}$$

Note that $\mathbf{curl}(Id - \mathbf{\Pi}_h)\mathbf{\Psi}_h$ is piecewise constant with vanishing flux through all triangular faces of $\mathcal{M}$. Then Stokes' theorem teaches that $\mathbf{curl}(Id - \mathbf{\Pi}_h)\mathbf{\Psi}_h = 0$.

By the projector property of $\mathbf{\Pi}_h$, $(Id - \mathbf{\Pi}_h)\mathbf{\Psi}_h$ satisfies the assumptions of Lemma 2.3. Taking into account that, moreover, the field is piecewise linear, it is clear that $(Id-\mathbf{\Pi}_h)\mathbf{\Psi}_h = \mathbf{grad}\psi$ with $\psi \in V_2(\mathcal{M})$. Along an arbitrary edge path γ in $\mathcal{M}$ we have

$$\int_\gamma (Id - \mathbf{\Pi}_h)\mathbf{\Psi}_h \cdot \mathrm{d}\vec{s} = 0$$

so that ψ attains the same value (w.l.o.g. $= 0$) on all vertices of $\mathcal{M}$. The stability of the splitting is a consequence of (2.23). □

By definition, the spaces $\mathbf{U}(\mathcal{M})$ and $V(\mathcal{M})$ accommodate the homogeneous boundary conditions on Γ_D. Later, we will also need finite element spaces oblivious of boundary conditions, that is, for the case $\Gamma_D = \emptyset$. These will be tagged by a bar on top, e.g., $\overline{\mathbf{U}}(\mathcal{M})$, $\overline{V}(\mathcal{M})$, etc. The same convention will be employed for notions and operators associated with finite element spaces: if they refer to the particular case $\Gamma_D = \emptyset$, they will be endowed with an overbar, e.g. $\overline{\mathbf{\Pi}}_h$, $\overline{\mathcal{I}}_h$, $\overline{\mathfrak{B}}_{\mathbf{U}}(\mathcal{M})$, $\overline{\mathcal{N}}(\mathcal{M})$, etc.

2.2. Meshes with Hanging Nodes

Now, general tetrahedral meshes *with hanging nodes* are admitted. We simply retain the definitions (2.8) and (2.19) of the spaces $V(\mathcal{M})$ and $V_2(\mathcal{M})$ of continuous finite element functions. Degrees of freedom for $V(\mathcal{M})$ are point evaluations at *active vertices* of $\mathcal{M}$. A vertex is called active, if it is not located in the interior of an edge/face of $\mathcal{M}$ or on Γ_D. A 2D[1)] illustration is given in Fig. 2.1.

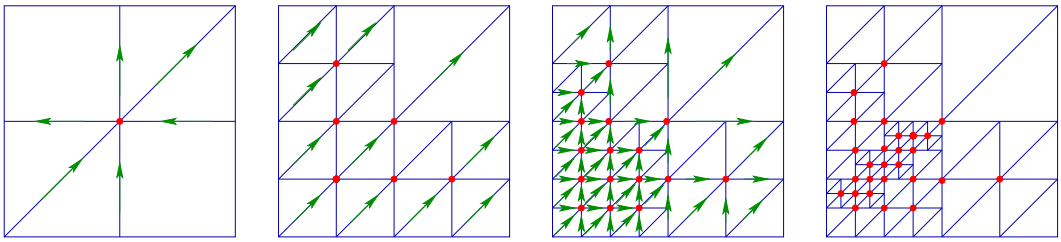

Fig. 2.1. Active vertices (red•) of 2D triangular meshes with hanging nodes, $\Omega =]0,1[^2$, $\Gamma_D = \partial\Omega$. In $\mathcal{M}_1, \mathcal{M}_2, \mathcal{M}_3$ active edges are marked with green arrows.

The values of a finite element function at the remaining ("slave") vertices are determined by recursive affine interpolation. A dual nodal basis $\mathfrak{B}_V(\mathcal{M})$ and corresponding interpolation operator $\mathcal{I}_h$ can be defined as above.

In principle, the definition (2.1) of the edge element space could be retained on non-conforming meshes, as well. Yet, for this choice an edge interpolation operator $\mathbf{\Pi}_h$ that satisfies the commuting diagram property (2.11) is not available. Thus, we construct basis functions directly and rely on the notion of *active edges*, see Fig. 2.1.

Definition 2.1. *An edge of $\mathcal{M}$ is* active, *if it is an edge of some $K \in \mathcal{M}$, not contained in Γ_D, and connects two vertices that are either active or located on Γ_D.*

[1)] For ease of visualization, we will often elucidate geometric concepts in two-dimensional settings. Their underlying ideas are the same in 2D and 3D.

We keep the symbol $\mathcal{E}(\mathcal{M})$ to designate the set of active edges of $\mathcal{M}$. To each $E \in \mathcal{E}(\mathcal{M})$ we associate a basis function $\mathbf{b}_E$, which, locally on the tetrahedra of $\mathcal{M}$, is a polynomial of the form (2.2). In order to fix this basis function completely, it suffices to speficify its path integrals (2.3) along *all* edges of $\mathcal{M}$. In the spirit of duality, we demand

$$\int_F \mathbf{b}_E \cdot \mathrm{d}\vec{s} = \begin{cases} 1, & \text{if } F = E \ , \\ 0, & \text{if } F \in \mathcal{E}(\mathcal{M}) \setminus \{E\} \ . \end{cases} \tag{2.25}$$

For the non-active ("slave") edges of $\mathcal{M}$ the path integrals of $\mathbf{b}_E$ (subsequently called "weights") are chosen to fit (2.11), keeping in mind that $\mathfrak{B}_{\mathbf{U}}(\mathcal{M}) := \{\mathbf{b}_E\}_{E\in\mathcal{E}(\mathcal{M})}$, and that the d.o.f. and $\mathbf{\Pi}_h$ are still defined according to (2.3) and (2.7), respectively. Ultimately, we set $\mathbf{U}(\mathcal{M}) :=$ Span $\{\mathfrak{B}_{\mathbf{U}}(\mathcal{M})\}$.

Let us explain the policy for setting the weights in the case of the subdivided tetrahedron of Fig. 2.2 with hanging nodes at the midpoints of edges, which will turn out to be the only relevant situation, *cf.* Sect. 5.1.

Weights have to be assigned to the "small edges" of the refined tetrahedron, some of which will be active, and some of which will have "slave" status, see the caption of Fig. 2.2.

We write the direction vectors of slave edges as linear combinations of active edges, for instance,

$$\begin{aligned} \boldsymbol{q}_1 - \boldsymbol{p}_3 &= \tfrac{1}{2}(\boldsymbol{p}_4 - \boldsymbol{p}_3) \ , \\ \boldsymbol{q}_1 - \boldsymbol{q}_2 &= \tfrac{1}{2}(\boldsymbol{p}_4 + \boldsymbol{p}_3) - \tfrac{1}{2}(\boldsymbol{p}_2 + \boldsymbol{p}_3) = \tfrac{1}{2}(\boldsymbol{p}_4 - \boldsymbol{p}_2) \ , \\ \boldsymbol{p}_5 - \boldsymbol{q}_4 &= \boldsymbol{p}_5 - \tfrac{1}{2}(\boldsymbol{p}_1 + \boldsymbol{p}_3) = \boldsymbol{p}_5 - \boldsymbol{p}_1 + \tfrac{1}{2}(\boldsymbol{p}_1 - \boldsymbol{p}_3) \ , \\ \boldsymbol{q}_4 - \boldsymbol{q}_3 &= \tfrac{1}{2}(\boldsymbol{p}_1 + \boldsymbol{p}_3) - \tfrac{1}{2}(\boldsymbol{p}_4 + \boldsymbol{p}_2) = \tfrac{1}{2}(\boldsymbol{p}_1 - \boldsymbol{p}_2) + \tfrac{1}{2}(\boldsymbol{p}_3 - \boldsymbol{p}_4) \ . \end{aligned}$$

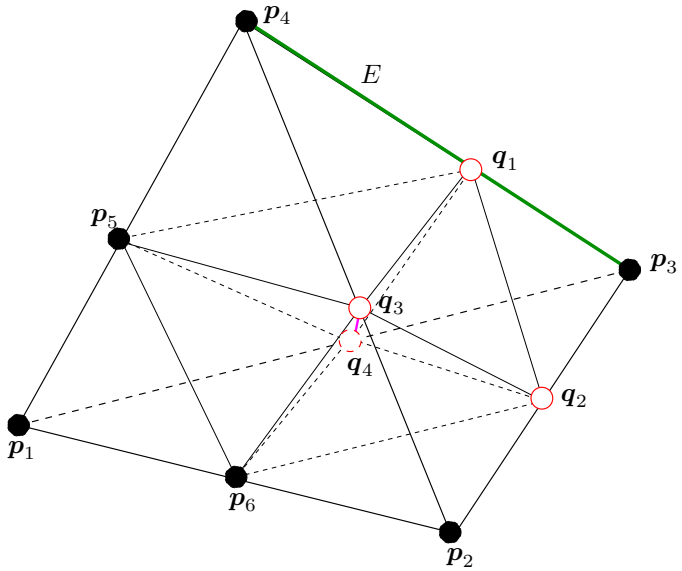

Fig. 2.2. Subdivided tetrahedron, active vertices (•) $\boldsymbol{p}_1, \ldots, \boldsymbol{p}_6$, slave vertices (redo) $\boldsymbol{q}_1, \ldots, \boldsymbol{q}_4$, active edges $[\boldsymbol{p}_1, \boldsymbol{p}_5]$, $[\boldsymbol{p}_1, \boldsymbol{p}_6]$, $[\boldsymbol{p}_4, \boldsymbol{p}_5]$, $[\boldsymbol{p}_2, \boldsymbol{p}_6]$, $[\boldsymbol{p}_2, \boldsymbol{p}_3]$, $[\boldsymbol{p}_2, \boldsymbol{p}_4]$, $[\boldsymbol{p}_3, \boldsymbol{p}_4]$, $[\boldsymbol{p}_5, \boldsymbol{p}_6]$, $[\boldsymbol{p}_1, \boldsymbol{p}_3]$, slave edges $[\boldsymbol{p}_1, \boldsymbol{q}_4]$, $[\boldsymbol{q}_4, \boldsymbol{p}_3]$, $[\boldsymbol{p}_2, \boldsymbol{q}_2]$, $[\boldsymbol{q}_2, \boldsymbol{p}_3]$, $[\boldsymbol{p}_3, \boldsymbol{q}_1]$, $[\boldsymbol{q}_1, \boldsymbol{p}_4]$, $[\boldsymbol{p}_6, \boldsymbol{q}_4]$, $[\boldsymbol{q}_2, \boldsymbol{q}_4]$, $[\boldsymbol{p}_6, \boldsymbol{q}_2]$, $[\boldsymbol{q}_1, \boldsymbol{q}_2]$, $[\boldsymbol{q}_2, \boldsymbol{q}_3]$, $[\boldsymbol{q}_1, \boldsymbol{q}_3]$, $[\boldsymbol{q}_1, \boldsymbol{p}_5]$, $[\boldsymbol{q}_3, \boldsymbol{p}_5]$, $[\boldsymbol{q}_4, \boldsymbol{p}_5]$

In a sense, we express slave edges as "linear combinations" of active edges. In a different context, this policy is explained in more detail in [24].

The coefficients in the combinations tell us the weights. For example, for the active edge $E = [\boldsymbol{p}_3, \boldsymbol{p}_4]$ in Fig. 2.2 they are given in Table 2.1. Using these weights and the formula (2.4), $\mathbf{b}_E$ can be assembled on the tetrahedron by imposing (see Table 2.1 for notations)

$$\int_S \mathbf{b}_E \cdot \mathrm{d}\vec{s} = \begin{cases} w_S & \text{for any contributing slave edge } S\,, \\ 0 & \text{for all other (slave) edges,} \end{cases} \qquad S \in \{\text{"small edges"}\}\,.$$

Table 2.1: Weights for slave edges in Fig. 2.2 relative to active edge $E = [\boldsymbol{p}_3, \boldsymbol{p}_4]$. Only slave edges with non-zero weights are listed.

Slave edge S	$[\boldsymbol{q}_1, \mathbf{p}_4]$	$[\boldsymbol{p}_3, \boldsymbol{q}_1]$	$[\boldsymbol{q}_2, \boldsymbol{q}_3]$	$[\boldsymbol{q}_4, \boldsymbol{p}_5]$	$[\boldsymbol{q}_3, \boldsymbol{q}_4]$
weight w_S	$\frac{1}{2}$	$\frac{1}{2}$	$\frac{1}{2}$	$\frac{1}{2}$	$-\frac{1}{2}$

Firstly, the procedure for the selection of weight guarantees that $\mathbf{grad}V(\mathcal{M}) \subset \mathbf{U}(\mathcal{M})$. For illustration, we single out the gradient $\mathbf{w}_h$ of the nodal basis function belonging to vertex $\boldsymbol{p}_5$ in Fig. 2.2. Its path integral equals 1 along the (oriented) edges $[\boldsymbol{p}_1, \boldsymbol{p}_5], [\boldsymbol{p}_3, \boldsymbol{p}_5], [\boldsymbol{p}_6, \boldsymbol{p}_5], [\boldsymbol{q}_4, \boldsymbol{p}_5], [\boldsymbol{q}_3, \boldsymbol{p}_5], [\boldsymbol{q}_1, \boldsymbol{p}_5]$, and vanishes on all other edges. Hence we expect

$$\mathbf{w}_h = \mathbf{b}_{[\boldsymbol{p}_1, \boldsymbol{p}_5]} + \mathbf{b}_{[\boldsymbol{p}_3, \boldsymbol{p}_5]} + \mathbf{b}_{[\boldsymbol{p}_6, \boldsymbol{p}_5]}\,. \tag{2.26}$$

This can be verified through showing equality of path integrals along slave edges. We take a close look at the slave edge $[\boldsymbol{q}_4, \boldsymbol{p}_5]$. By construction the basis functions belonging to active edges satisfy

$$\begin{aligned} &\int_{[\boldsymbol{q}_4, \boldsymbol{p}_5]} \mathbf{b}_{[\boldsymbol{p}_1, \boldsymbol{p}_5]} \cdot \mathrm{d}\vec{s} = 1\,, \quad \int_{[\boldsymbol{q}_4, \boldsymbol{p}_5]} \mathbf{b}_{[\boldsymbol{p}_5, \boldsymbol{p}_4]} \cdot \mathrm{d}\vec{s} = 0\,, \quad \int_{[\boldsymbol{q}_4, \boldsymbol{p}_5]} \mathbf{b}_{[\boldsymbol{p}_3, \boldsymbol{p}_4]} \cdot \mathrm{d}\vec{s} = 0\,, \\ &\int_{[\boldsymbol{q}_4, \boldsymbol{p}_5]} \mathbf{b}_{[\boldsymbol{p}_1, \boldsymbol{p}_3]} \cdot \mathrm{d}\vec{s} = -\tfrac{1}{2}\,, \quad \int_{[\boldsymbol{q}_4, \boldsymbol{p}_5]} \mathbf{b}_{[\boldsymbol{p}_1, \boldsymbol{p}_6]} \cdot \mathrm{d}\vec{s} = 0\,, \\ &\int_{[\boldsymbol{q}_4, \boldsymbol{p}_5]} \mathbf{b}_{[\boldsymbol{p}_2, \boldsymbol{p}_6]} \cdot \mathrm{d}\vec{s} = 0\,, \quad \int_{[\boldsymbol{q}_4, \boldsymbol{p}_5]} \mathbf{b}_{[\boldsymbol{p}_2, \boldsymbol{p}_3]} \cdot \mathrm{d}\vec{s} = 0\,. \end{aligned}$$

Then, evidently,

$$\begin{aligned} 1 &= \int_{[\boldsymbol{q}_4, \boldsymbol{p}_5]} \mathbf{w}_h \cdot \mathrm{d}\vec{s} \\ &= \int_{[\boldsymbol{q}_4, \boldsymbol{p}_5]} \mathbf{b}_{[\boldsymbol{p}_1, \boldsymbol{p}_5]} \cdot \mathrm{d}\vec{s} + \int_{[\boldsymbol{q}_4, \boldsymbol{p}_5]} \mathbf{b}_{[\boldsymbol{p}_3, \boldsymbol{p}_5]} \cdot \mathrm{d}\vec{s} + \int_{[\boldsymbol{q}_4, \boldsymbol{p}_5]} \mathbf{b}_{[\boldsymbol{p}_6, \boldsymbol{p}_5]} \cdot \mathrm{d}\vec{s} = 1 + 0 + 0\,. \end{aligned}$$

The same considerations apply to all other slave edges and (2.26) is established. Secondly, the construction ensures the commuting diagram property (2.11): again appealing to Fig. 2.2 we find, for example,

$$\begin{aligned}
&\int\limits_{[\boldsymbol{q}_3,\boldsymbol{q}_4]} \mathbf{grad}\mathcal{I}_h u \cdot \mathrm{d}\vec{s} = \mathcal{I}_h u(\boldsymbol{q}_4) - \mathcal{I}_h u(\boldsymbol{q}_3) \\
&= \tfrac{1}{2}(u(\boldsymbol{p}_4) + u(\boldsymbol{p}_2)) - \tfrac{1}{2}(u(\boldsymbol{p}_1) + u(\boldsymbol{p}_3)) \\
&= \tfrac{1}{2} \int\limits_{[\boldsymbol{p}_3,\boldsymbol{p}_4]} \mathbf{grad} u \cdot \mathrm{d}\vec{s} + \tfrac{1}{2} \int\limits_{[\boldsymbol{p}_1,\boldsymbol{p}_2]} \mathbf{grad} u \cdot \mathrm{d}\vec{s} \\
&= \tfrac{1}{2} \int\limits_{[\boldsymbol{p}_3,\boldsymbol{p}_4]} \mathbf{grad} u \cdot \mathrm{d}\vec{s} + \tfrac{1}{4} \int\limits_{[\boldsymbol{p}_1,\boldsymbol{p}_6]} \mathbf{grad} u \cdot \mathrm{d}\vec{s} + \tfrac{1}{4} \int\limits_{[\boldsymbol{p}_6,\boldsymbol{p}_2]} \mathbf{grad} u \cdot \mathrm{d}\vec{s}\,.
\end{aligned}$$

In words, combining the path integrals of $\mathbf{grad}u$ along active edges with the relative weights of the slave edge $[\boldsymbol{q}_3, \boldsymbol{q}_4]$ yields the same result as evaluating the path integral of the gradient of the interpolant $\mathcal{I}_h u$ along $[\boldsymbol{q}_3, \boldsymbol{q}_4]$.

The definitions (2.19) and (2.20) also carry over to meshes with hanging nodes. This remains true for the splitting asserted in Lemma 2.2. However, though the algebraic relationships like (2.11) remain valid, the estimates and norm equivalences of the previous section do not hold for general families of meshes with hanging nodes. This entails restrictions on the location of hanging nodes, whose discussion will be postponed until Sect. 3.2, *cf.* Assumption 3.1.

Remark 2.1. Our presentation is confined to tetrahedral meshes and lowest order edge elements for the sake of simplicity. Extension of all results to hexahedral meshes and higher order edge elements is possible, but will be technical and tedious.

3. Local Mesh Refinement

We study the case where the actual finite element mesh $\mathcal{M}_h$ of Ω has been created by successive local refinement of a relatively uniform initial mesh $\mathcal{M}_0$. Concerning $\mathcal{M}_h$ and $\mathcal{M}_0$ the following *asumptions* will be made:

1. Given $\mathcal{M}_0$ and $\mathcal{M}_h$ we can construct a *virtual* refinement hierarchy of $L+1$ *nested*[1)] tetrahedral meshes, $L \in \mathbb{N}$:
$$\mathcal{M}_0 \prec \mathcal{M}_1 \prec \mathcal{M}_2 \prec \cdots \prec \mathcal{M}_L = \mathcal{M}_h\,. \tag{3.1}$$
Please note that the virtual refinement hierarchy may be different from the actual sequence of meshes spawned during adaptive refinement[2)] .
2. Inductively, we assign to each tetrahedron $K \in \mathcal{M}_l$ a level $\ell(K) \in \mathbb{N}_0$ by counting the number of subdivisions it took to generate it from an element of $\mathcal{M}_0$.
3. For all $0 \le l < L$ the mesh $\mathcal{M}_{l+1}$ is created by subdividing some or all of the tetrahedra in $\{K \in \mathcal{M}_l : \ell(K) = l\}$.
4. The shape regularity measures of the meshes $\mathcal{M}_l$ are uniformly bounded independently of L.

[1)] two finite element meshes $\mathcal{M}$ and $\mathcal{T}$ are nested, $\mathcal{M} \prec \mathcal{T}$, if every element of $\mathcal{M}$ is the union of elements of $\mathcal{T}$. [2)] For the local multigrid algorithm examined in this article the implementation must provide access to the virtual refinement hierarchy. This entails suitable bookkeeping data structures, which are available in the ALBERTA package used for the numerical experiments in Sect. 6

Refinement may be local, but it must be regular in the following sense, *cf.* [39, Sect. 4.2.2] and [52]: we can find a second sequence of nested tetrahedral meshes of Ω

$$\mathcal{M}_0 = \widehat{\mathcal{M}}_0 \prec \widehat{\mathcal{M}}_1 \prec \widehat{\mathcal{M}}_2 \prec \cdots \prec \widehat{\mathcal{M}}_L \tag{3.2}$$

that satisfies

1. $\mathcal{M}_l \prec \widehat{\mathcal{M}}_l$ and $\{K \in \mathcal{M}_l : \ell(K) = l\} \subset \widehat{\mathcal{M}}_l$, $l = 0, \ldots, L$,
2. that the shape regularity measure $\rho_{\widehat{\mathcal{M}}_l}$ is bounded independently of l,
3. and that there exist two constants $C > 0$ and $0 < \theta < 1$ independent of l and L such that

$$C^{-1}\theta^l \le h_K \le C\theta^l \quad \forall K \in \widehat{\mathcal{M}}_l\,, \quad 0 \le l \le L\,. \tag{3.3}$$

This means that the family $\{\widehat{\mathcal{M}}_l\}_l$ is quasi-uniform. Hence, it makes sense to refer to a mesh width $h_l := \max\{h_K,\, K \in \widehat{\mathcal{M}}_l\}$ of $\widehat{\mathcal{M}}_l$. It decreases geometrically for growing l.

Our analysis targets two popular tetrahedral refinement schemes that generate sequences of meshes that meet the above requirements.

3.1. Local regular refinement

This scheme produces $\mathcal{M}_{l+1}$ by splitting some of the tetrahedra of the current mesh $\mathcal{M}_l$ into eight smaller ones, possibly creating hanging nodes in the process [1]. An illustrative 2D example with hanging nodes is depicted in Figure 3.1. The accompanying sequence $\{\widehat{\mathcal{M}}_l\}_{0\le l\le L}$ is produced by global regular refinement, which implies (3.3) with $\theta = \frac{1}{2}$. Uniform shape-regularity can also be guaranteed for repeated regular refinement of tetrahedra, see [9].

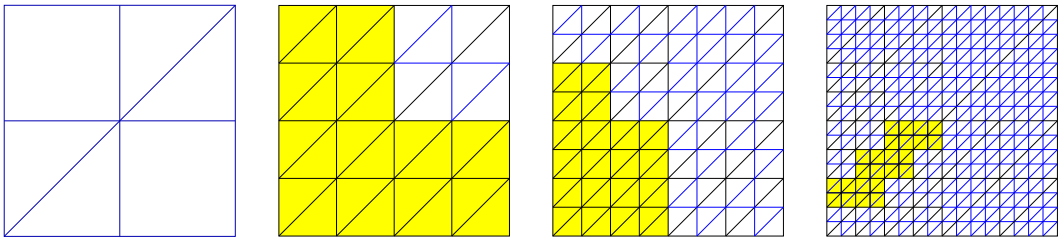

$\mathcal{M}_0$ $\mathcal{M}_1$ $\mathcal{M}_2$ $\mathcal{M}_3 = \mathcal{M}_h$

Fig. 3.1. Virtual refinement hierarchy for 2D triangular meshes. The quasi-uniform sequence $\{\widehat{\mathcal{M}}_l\}_{0\le l\le L}$ is sketched in blue. Elements of $\mathcal{M}_l$ eligible for further subdivision are marked yellow.

The meshes occurring in the virtual refinement hierarchy need not agree with the meshes that arise during adaptive refinement in an actual computation. Yet, given $\mathcal{M}_h$, the virtual refinement hierarchy can always be found *a posteriori*. Write $\mathcal{M}_{\rm hier}$ for the union of all tetrahedra ever created during the refinement process. Then, for $0 < l < L$, define

$$\mathcal{M}_l := \left\{ K \in \mathcal{M}_{\rm hier} : \begin{array}{l} \ell(K) \le l \quad \text{and } K \text{ does not contain a} \\ K' \in \mathcal{M}_{\rm hier} \setminus \{K\} \text{ with } \ell(K') \le l \end{array} \right\}. \tag{3.4}$$

Using the construction of finite element spaces detailed in Sect. 2.2, the local multigrid algorithms can handle any kind of local regular refinement. Yet, convergence may degrade unless we curb extreme jumps of local meshwidth. Thus, we assume the following throughout the remainder of this paper.

Assumption 3.1. *Any edge of $\mathcal{M}_h$ may contain at most one hanging node.*

This will automatically be satisfied for all meshes $\mathcal{M}_l$ of the virtual refinement hierarchy. Consequently, hanging nodes can occur only in a few geometric configurations, one of which is depicted in Fig. 2.2. This paves the way for using mapping techniques and scaling arguments, see [26, Sect. 3.6], which confirm the following generalization of results of Sect. 2.1. Of course, we rely on the constructions of finite element spaces and interpolation operators described in Sect. 2.2.

Proposition 3.1. *Under Assumption* 3.1 *the L^2-stability of bases, see* (2.6) *and* (2.9)*, carries over uniformly to meshes created by local regular refinement. So do Lemmas* 2.1 *and* 2.2*, and Estimates* (2.22) *and* (2.23)*.*

Summing up, Assumption 3.1 makes it possible to use the results obtained in Sect. 2.1 in the case of local regular refinement as well. To avoid a proliferation of labels, we are going to quote the statements from Sect. 2.1 even when we mean their generalization to meshes with hanging nodes.

3.2. Recursive bisection refinement

This procedure involves splitting a tetrahedron into two by promoting the midpoint of the so-called refinement edge to a new vertex. Variants of bisection differ by the selection of refinement edges: The iterative bisection strategy by Bänsch [4, 6] needs the intermediate handling of hanging nodes. The recursive bisection strategies of [33, 34, 49] do not create such hanging nodes and, therefore, are easier to implement. But for special $\mathcal{M}_0$, the two recursive algorithms result in exactly the same tetrahedral meshes as the iterative algorithm. Since our implementation relies on the bisection algorithm of [33], we outline its bisection policy in the following. For more information on bisection algorithms, we refer to [42, 48].

For the recursive bisection algorithm of [33], the bisections of tetrahedra are totally determined by the local vertex numbering of $\mathcal{M}_0$, plus a prescribed type for every element in $\mathcal{M}_0$. Each tetrahedron K is endowed with the local indices 0, 1, 2, and 3 for its vertices. The refinement edge of each element is always set to be the edge connecting vertex 0 and vertex 1. After bisection of K, the "child tetrahedron" of K which contains vertex 0 of K is denoted by Child[0] and the other one is denoted by Child[1]. The types of Child[0] and Child[1] are defined by

$$\mathsf{type}(\text{Child}[0]) = \mathsf{type}(\text{Child}[1]) = (\mathsf{type}(K) + 1) \mod 3.$$

The new vertex at the midpoint of the refinement edge of K is always numbered by 3 in Child[0] and Child[1]. The four vertices of K are numbered in Child[0] and Child[1] as follows (see Fig. 3.2):

$$\begin{aligned}
&\text{In Child}[0]: && (0,2,3) \to (0,1,2), && \\
&\text{In Child}[1]: && (0,2,3) \to (0,2,1), && \text{if} \quad \mathsf{type}(K) = 0, \\
&\text{In Child}[1]: && (0,2,3) \to (0,1,2), && \text{if} \quad \mathsf{type}(K) > 0.
\end{aligned}$$

This recursive bisection creates only a small number of similarity classes of tetrahedra, see [33, 42, 49].

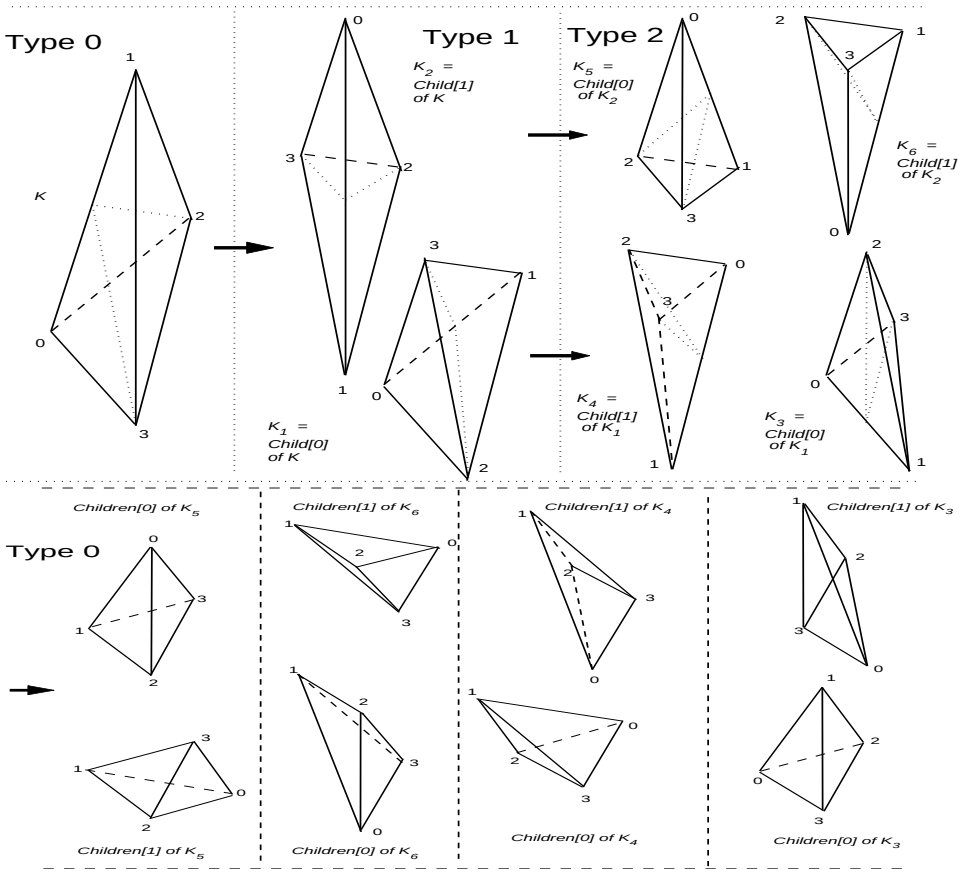

Fig. 3.2. Bisection of tetrahedra in the course of recursive bisection. Assignment of types to children

Fig 3.3 shows a 2D example of the recursive bisection refinement (the algorithm for 2D case is called "the newest vertex bisection" in [36]). Similar to the 3D algorithm, for any element K, its three vertices are locally numbered by 0, 1, and 2, its refinement edge is the edge between vertex 0 and 1. The newly created vertex in the two children of K are numbered by 2. In the child element containing vertex 0 of K, vertex 0 and 2 of K are renumbered by 1 and 0 respectively. In the other child element, vertex 1 and 2 of K are renumbered by 0 and 1 respectively.

In order to keep the mesh conforming during refinements, the bisection of an edge is only allowed when such an edge is the refinement edge for all elements which share this edge. If a tetrahedron has to be refined, we have to loop around its refinement edge and collect all elements at this edge to create an refinement patch. Then this patch is refined by bisecting the common refinement edge. A more detailed discussion can be found in [33].

For any mesh $\mathcal{M}_l$ an associated "quasi-uniform" mesh $\widehat{\mathcal{M}}_l$ according to (3.2), $\mathcal{M}_l \prec \widehat{\mathcal{M}}_l$, is obtained as follows: the elements in $\{K \in \mathcal{M}_l : \ell(K) < l\}$ undergo bisection until $\ell(K) = l$ for any $K \in \widehat{\mathcal{M}}_l$.

We still have to make sure that the recursive bisection allows the definition of a virtual

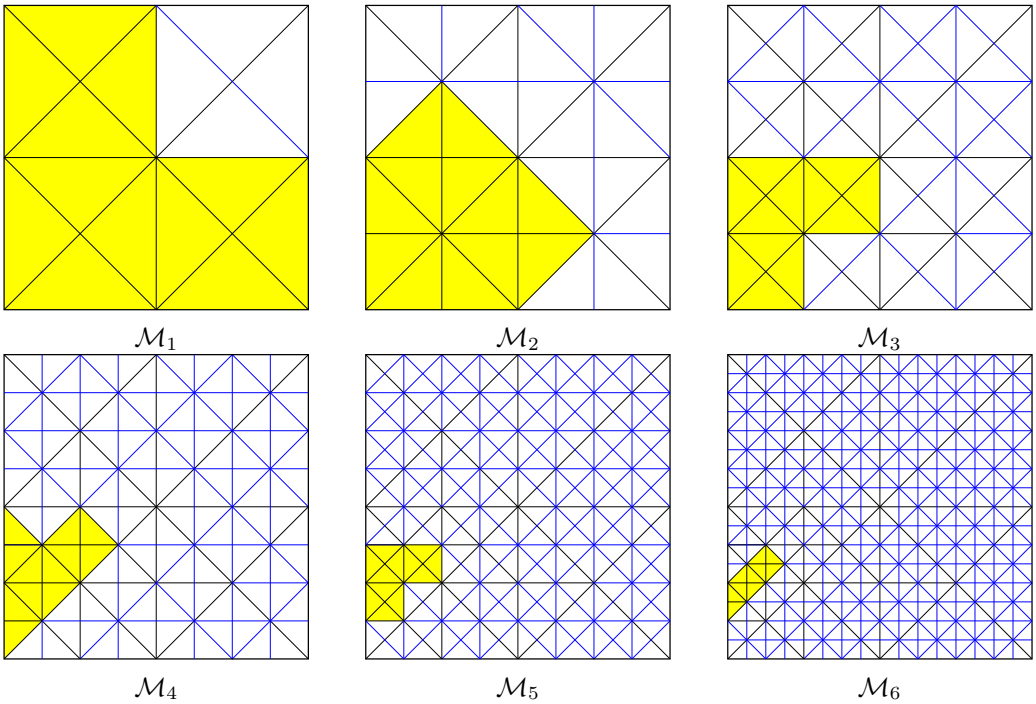

Fig. 3.3. Virtual refinement hierarchy for 2D triangular meshes emerging in the course of successive local newest vertex bisection refinement of $\mathcal{M}_0$ from Fig. 3.1. Accompanying quasi-uniform meshes outlined in blue, maximally refined triangles marked yellow.

refinement hierarchy. Thus, let $\mathcal{M}_h = \mathcal{M}_L$ be generated from the initial mesh $\mathcal{M}_0$ by the bisection algorithm in [33]. Denote by $\mathcal{M}_{\text{hier}}$ the set of all tetrahedra created during the bisection process, i.e., for any $K \in \mathcal{M}_{\text{hier}}$, there is a $K' \in \mathcal{M}_h$ such that either $K' = K$ or K' is created by refining K. Then, the virtual meshes $\mathcal{M}_l$, $0 < l < L$ can again be defined according to (3.4).

In the following, we are going to prove that each $\mathcal{M}_l$ is a conforming mesh, that is, no hanging nodes occur in $\mathcal{M}_l$, $0 \le l \le L$. The proof depends on some mild assumptions on $\mathcal{M}_0$ (see assumptions (A1) and (A2) in [33]), which will be taken for granted.

Lemma 3.1. [33, *Lemmas* 2,3] *Let $T, T' \in \mathcal{M}_h$ be a pair of tetrahedra sharing a face $F = K \cap K'$. It holds true that*

1. *if T contains the refinement edge of T' and vice versa, then they have the same refinement edge,*
2. *if F contains the refinement edges of both K and K', then $\ell(K) = \ell(K')$,*
3. *if F contains the refinement edge of K, but does not contain the refinement edge of K', then $\ell(K) = \ell(K') + 1$,*
4. *if F does not contain the refinement edges of K and K', then $\ell(K) = \ell(K')$.*

Lemma 3.2. *The meshes $\mathcal{M}_l$, $0 \le l \le L$, according to* (3.4) *are conforming meshes.*

Proof. We are going to prove the lemma by backward induction starting from $l = L$. Since $\mathcal{M}_L = \mathcal{M}_h$ is conforming, for any $K \in \mathcal{M}_L$ satisfying $\ell(K) = L$, there exists a brother of K,

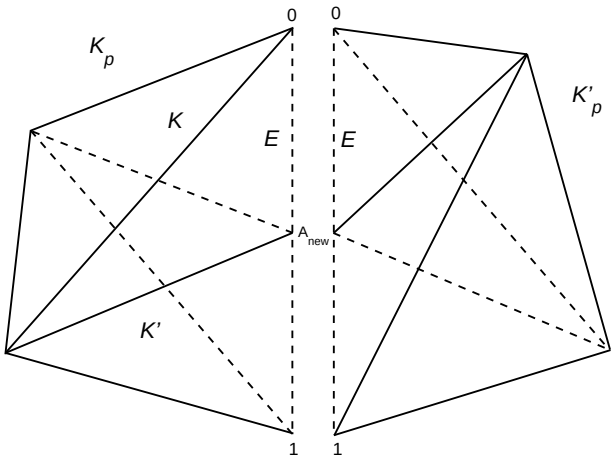

Fig. 3.4. The patch around a refinement edge E with vertex 0 and 1. $\ell(K) = \ell(K') = L$ and $\ell(K_p) = \ell(K'_p) = L - 1$.

denoted by $K' \in \mathcal{M}_L$, such that $\ell(K') = L$ and $K_p := K \cup K' \in \mathcal{M}_{L-1}$. Here K_p is called the parent of K and K' with $\ell(K_p) = L - 1$ (see Fig. 3.4).

Let E be the refinement edge of K_p. By the recursive bisection algorithm, E must be the common refinement edge of all tetrahedra in the refinement patch:

$$P_E = \bigcup \{\, \overline{K'_p} : \; K'_p \in \mathcal{M}_{L-1} \text{ and } E \subset \overline{K'_p} \,\}.$$

By Lemma 3.1, $\ell(K'_p) = L - 1$ for any $K'_p \subset P_E$ and the midpoint of E, denoted by A_{new}, is the unique new vertex of $\mathcal{M}_L$ in P_E. We conclude that

$$P_E = \bigcup \{\, \overline{K} : \; K \in \mathcal{M}_L, \; \ell(K) = L, \text{ and } A_{\text{new}} \text{ is a vertex of } K \,\}.$$

Coarsen the sub-mesh $\mathcal{M}_{L|P_E}$ by removing the vertex A_{new} and all edges related to it and adding E to this patch. Thus a conforming sub-mesh $\mathcal{M}_{L-1|P_E}$ is obtained. Do the above coarsening process for every element $K \in \mathcal{M}_L$ with $\ell(K) = L$. This proves that $\mathcal{M}_{L-1}$ is conforming.

Finally, an induction argument confirms that $\mathcal{M}_l$ is conforming, $l = L - 2, \cdots, 1$. □

4. Local Multigrid

To begin with, we introduce nested refinement zones as open subsets of Ω:

$$\omega_l := \text{interior}\Big(\bigcup \{ \overline{K} : \; K \in \mathcal{M}_h, \, \ell(K) \geq l \} \Big) \subset \Omega \,, \tag{4.1}$$

see Fig. 4.1 and Fig. 4.2. The notion of refinement zones allows a concise definition of the local multilevel decompositions of the finite element spaces $V(\mathcal{M}_h)$ and $\mathbf{U}(\mathcal{M}_h)$ that underly the local multigrid method.

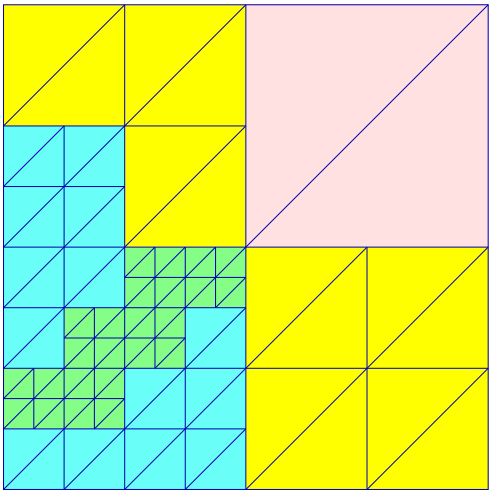

"Refinement strips": set differences of refinement zones

Fig. 4.1. Refinement zones for the 2D refinement hierarchy of Figure 3.1.

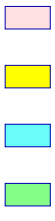

: $\Sigma_0 := \omega_0 \setminus \omega_1$

: $\Sigma_1 := \omega_1 \setminus \omega_2$

: $\Sigma_2 := \omega_2 \setminus \omega_3$

: $\Sigma_3 := \omega_3$

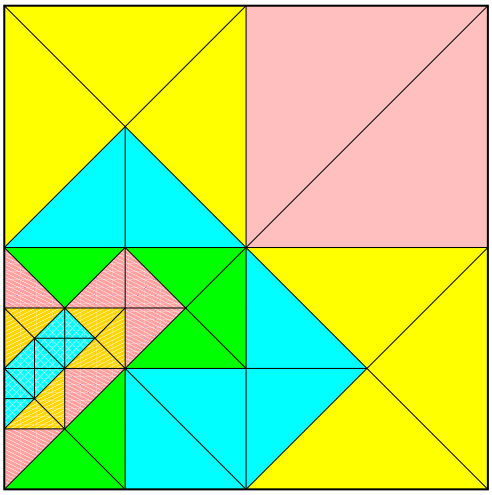

"Refinement strips": set differences of refinement zones

: $\Sigma_0 := \omega_0 \setminus \omega_1$

: $\Sigma_1 := \omega_1 \setminus \omega_2$

: $\Sigma_2 := \omega_2 \setminus \omega_3$

: $\Sigma_3 := \omega_3 \setminus \omega_4$

: $\Sigma_4 := \omega_4 \setminus \omega_5$

: $\Sigma_5 := \omega_5 \setminus \omega_6$

: $\Sigma_6 := \omega_6$

Fig. 4.2. Refinement zones for the 2D refinement hierarchy of Figure 3.3.

We introduce local multigrid from the perspective of multilevel successive subspace correction (SSC) [53, 54, 56]. First, we give an abstract description for a linear variational problem

$$u \in H : \quad \mathsf{a}(u,v) = f(v) \quad \forall v \in H \ , \tag{4.2}$$

involving a positive definite bilinear form a on a Hilbert space H. The method is completely defined after we have provided a finite subspace decomposition

$$H = \sum_{j=0}^{J} H_j \ , \quad H_j \subset H \text{ closed subspaces, } j = 0, \ldots, J, \ J \in \mathbb{N} \ . \tag{4.3}$$

Then the correction scheme implementation of one step of SSC acting on the iterate u^{m-1} reads:

for $m = 1, 2, \cdots$

$u_{-1}^{m-1} = u^{m-1}$

for $j = 0, 1, \cdots, J$

Let $e_j \in H_j$ solve

$$\mathsf{a}(e_j, v_j) = f(v_j) - \mathsf{a}(u_{j-1}^{m-1}, v_j) \quad \forall\, v_j \in H_j$$

$u_j^{m-1} = u_{j-1}^{m-1} + e_j$

endfor

$u^m = u_J^{m-1}$

endfor

This amounts to a stationary linear iterative method with error propagation operator

$$E = (I - P_J)(I - P_{J-1}) \cdots (I - P_0)\ , \tag{4.4}$$

where $P_j : H \mapsto H_j$ stands for the Galerkin projection defined through

$$\mathsf{a}(P_j v, v_j) = \mathsf{a}(v, v_j) \quad \forall\, v_j \in H_j. \tag{4.5}$$

The convergence theory of SSC for an inner product a and induced energy norm $\|\cdot\|_A$ rests on two assumptions. The first one concerns the *stability of the space decomposition*. We assume that there exists a constant C_{stab} independent of J such that

$$\inf\Big\{ \sum_{j=0}^{J} \|v_j\|_A^2 :\ \sum_{j=0}^{J} v_j = v \Big\} \le C_{\mathrm{stab}} \|v\|_A^2 \quad \forall\, v \in H. \tag{4.6}$$

The second assumption is a *strengthened Cauchy-Schwartz inequality*, namely, there exist two constants $0 \le q < 1$ and C_{orth} independent of j and k such that

$$\mathsf{a}(v_j, v_k) \le C_{\mathrm{orth}} q^{|k-j|} \|v_j\|_A \|v_k\|_A \quad \forall\, v_j \in H_j,\ v_k \in H_k\ . \tag{4.7}$$

The above inequality states a kind of quasi-orthogonality between the subspaces. From [53, Theorem 4.4] and [57, Theorem 5.1] we cite the following central convergence theorem:

Theorem 4.1. *Provided that* (4.6) *and* (4.7) *hold, the convergence rate of Algorithm SSC is bounded by*

$$\|E\|_A^2 \le 1 - \frac{1}{C_{\mathrm{stab}}(1+\Theta)^2} \quad \textit{with} \quad \Theta = C_{\mathrm{orth}} \frac{1+q}{1-q}, \tag{4.8}$$

where the operator norm is defined by

$$\|E\|_A := \sup_{v \in H, v \neq 0} \frac{\|Ev\|_A}{\|v\|_A}.$$

The bottom line is that the subspace splitting (4.3) already provides a full description of the method. Showing that both constants C_{stab} from (4.6) and C_{orth} from (4.7) can be chosen independently of the number L of refinement levels is the challenge in asymptotic multigrid analysis.

In concrete terms, the role of the linear variational problem (4.2) is played by (1.1) considered on the edge element space $\mathbf{U}(\mathcal{M}_h)$, which replaces the Hilbert space H. To define the local multilevel decomposition of $\mathbf{U}(\mathcal{M}_h)$, we define "sets of new basis functions" on the various refinement levels

$$\begin{aligned} &\mathfrak{B}_V^0 := \mathfrak{B}_V(\mathcal{M}_0), \quad \mathfrak{B}_V^l := \{b_h \in \mathfrak{B}_V(\mathcal{M}_l) : \operatorname{supp} b_h \subset \overline{\omega}_l\} , \\ &\mathfrak{B}_{\mathbf{U}}^0 := \mathfrak{B}_{\mathbf{U}}(\mathcal{M}_0), \quad \mathfrak{B}_{\mathbf{U}}^l := \{\mathbf{b}_h \in \mathfrak{B}_{\mathbf{U}}(\mathcal{M}_l) : \operatorname{supp} \mathbf{b}_h \subset \overline{\omega}_l\} , \end{aligned} \quad 1 \le l \le L . \tag{4.9}$$

A 2D drawing of the sets $\mathfrak{B}_V^l$ is given in Fig. 4.3 where $\Gamma_D = \partial\Omega$. Note that we also have to deal with $V(\mathcal{M}_h)$, because, as suggested by the reasoning in [25], a local multilevel decomposition of $\mathbf{U}(\mathcal{M}_h)$ has to incorporate an appropriate local multilevel decomposition of $V(\mathcal{M}_h)$.

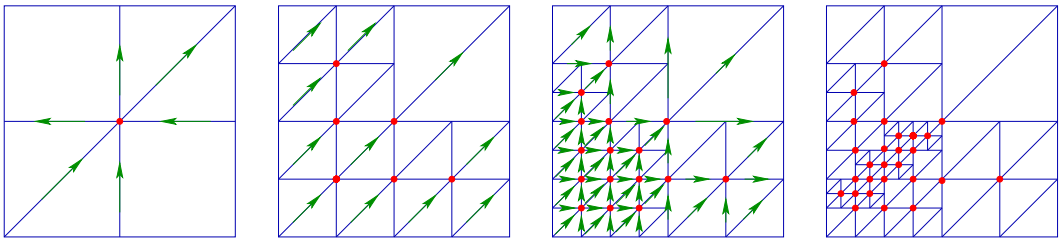

$l = 0$ $l = 1$ $l = 2$ $l = 3$

Fig. 4.3. Active vertices (redred) carrying "tent functions" in $\mathfrak{B}_V^l$, $\Gamma_D = \partial\Omega$, refinement hierarchy of Fig. 3.1

Then, a possible local multigrid iteration for the linear system of equations arising from a finite element Galerkin discretization of a $H^1_{\Gamma_D}(\Omega)$-elliptic variational problem boils down to a successive subspace correction method based on the local multilevel decomposition

$$V(\mathcal{M}_h) = V(\mathcal{M}_0) + \sum_{l=1}^{L} \sum_{b_h \in \mathfrak{B}_V^l} \operatorname{Span}\{b_h\} . \tag{4.10}$$

Similarly, the local multilevel splitting of $\mathbf{U}(\mathcal{M}_h)$ is based on the multilevel decomposition

$$\mathbf{U}(\mathcal{M}_h) = \mathbf{U}(\mathcal{M}_0) + \sum_{l=1}^{L} \sum_{b_h \in \mathfrak{B}_V^l} \operatorname{Span}\{\mathbf{grad} b_h\} + \sum_{l=1}^{L} \sum_{\mathbf{b}_h \in \mathfrak{B}_{\mathbf{U}}^l} \operatorname{Span}\{\mathbf{b}_h\} . \tag{4.11}$$

These splittings induce SSC iterations that can be implemented as non-symmetric multigrid V-cycles with only one (hybrid) Gauss-Seidel post-smoothing step, see [25, Sect. 6]. Duplicating components of (4.11) results in more general multigrid cycles with various numbers of pre- and post-smoothing steps.

The splitting (4.11) is motivated both by the design of multigrid methods for (1.1) and $\mathbf{U}(\mathcal{M})$ in the case of uniform refinement and local multigrid approaches to $H^1_{\Gamma_D}(\Omega)$-elliptic variational problems after discretization by means of linear finite elements [36, 52]. The occurrence of gradients of "tent functions" b_h in (4.11) is related to the *hybrid local relaxation*, which is essential for the performance of multigrid in $\boldsymbol{H}(\mathbf{curl}, \Omega)$, see [25] for a rationale. A rigorous

justification will emerge during the theoretical analysis in the following sections. It will establish the following main theorem.

Theorem 4.2 (Asymptotic convergence of local multigrid for edge elements) *Under the assumptions on the meshes made above and allowing at most one hanging node per edge, the decomposition* (4.11) *leads to an SSC iteration whose convergence rate is bounded away from* 1 *uniformly in the number L of refinement steps.*

Proving stability estimate (4.6) is the chief challenge, whereas the strengthened Cauchy-Schwarz inequality (4.7) for the local multilevel decomposition (4.11) is amenable to exactly the same proof as in the case of global refinement. The reader is referred to [27, Sect. 4] and [30, Sect. 6].

5. Stability

First we recall the stability estimate (4.6) for the local multilevel decomposition (4.10), which is implicitly contained in (4.11). Proofs can be found in [39, Ch. 4] and [30, Sect. 5].

Theorem 5.1. *For any $u_h \in V(\mathcal{M}_h)$ we can find $u_l \in V(\mathcal{M}_l)$ such that*

$$u_h = \sum_{l=0}^{L} u_l, \qquad \operatorname{supp}(u_l) \subset \overline{\omega}_l \;, \tag{5.1}$$

and

$$|u_0|^2_{H^1(\Omega)} + \sum_{l=1}^{L} h_l^{-2} \, \|u_l\|^2_{L^2(\Omega)} \leq C |u_h|^2_{H^1(\Omega)} \;,$$

with $C > 0$ independent of L.

Notice that in combination with the L^2-stability (2.9) of nodal bases and inverse inequalities, this theorem asserts an L-uniform estimate of the form (4.6) for the splitting (4.10) w.r.t. the energy norm $|\cdot|_{H^1(\Omega)}$. From (5.1) it is clear that the basis functions admitted in (4.10) can represent the functions u_l of Thm. 5.1.

5.1. Helmholtz-type decompositions

Helmholtz-type decompositions, also called *regular decompositions*, have emerged as a powerful tool for answering questions connected with $\boldsymbol{H}(\mathbf{curl}, \Omega)$. In particular, they have paved the way for a rigorous multigrid theory for $\boldsymbol{H}(\mathbf{curl}, \Omega)$-elliptic problems [17,23,25,27–29,32,40]. We refer to [26, Sect. 2.4] for more information.

We will need a very general version provided by the following theorem.

Theorem 5.2. *Let Ω meet the requirements stated in Sect.* 1. *Then, for any $\mathbf{v} \in \boldsymbol{H}_{\Gamma_D}(\mathbf{curl}, \Omega)$, there exists a $p \in H^1_{\Gamma_D}(\Omega)$ and $\boldsymbol{\Psi} \in (H^1_{\Gamma_D}(\Omega))^3$ such that*

$$\mathbf{v} = \nabla p + \boldsymbol{\Psi}, \tag{5.2}$$

$$|p|_{H^1(\Omega)} \leq C \|\mathbf{v}\|_{\boldsymbol{H}(\mathbf{curl},\Omega)}, \quad \|\boldsymbol{\Psi}\|_{H^1(\Omega)} \leq C \|\,\mathbf{curl}\,\mathbf{v}\|_{L^2(\Omega)}, \tag{5.3}$$

where the constant C depends only on Ω.

Proof. Given $\mathbf{u} \in \boldsymbol{H}_{\Gamma_D}(\mathbf{curl}, \Omega)$, we define $\widetilde{\mathbf{u}} \in \boldsymbol{H}(\mathbf{curl}, \widetilde{\Omega})$, $\widetilde{\Omega} := \text{interior}(\overline{\Omega} \cup \overline{\Omega}_1 \cup \overline{\Omega}_2 \cup \dots)$ (see Sect. 1 and Fig. 5.1 for the meaning of Ω_i), by

$$\widetilde{\mathbf{u}}(\boldsymbol{x}) = \begin{cases} \mathbf{u}(\boldsymbol{x}) & \text{for } \boldsymbol{x} \in \Omega \,, \\ 0 & \text{for } \boldsymbol{x} \in \Omega_i \text{ for some } i \,. \end{cases} \tag{5.4}$$

Notice that the tangential components of $\widetilde{\mathbf{u}}$ are continuous across $\partial\Omega$, which ensures $\widetilde{\mathbf{u}} \in \boldsymbol{H}(\mathbf{curl}, \widetilde{\Omega})$. Then extend $\widetilde{\mathbf{u}}$ to $\overline{\mathbf{u}} \in \boldsymbol{H}(\mathbf{curl}, \mathbb{R}^3)$, see [16].

Since $\mathbf{curl}\,\overline{\mathbf{u}} \in \boldsymbol{H}(\operatorname{div} 0, \mathbb{R}^3)$, Fourier techniques [22, Sect. 3.3] yield a $\boldsymbol{\Phi} \in (H^1(\mathbb{R}^3))^3$ that fulfills

$$\mathbf{curl}\,\boldsymbol{\Phi} = \mathbf{curl}\,\overline{\mathbf{u}} \,, \quad \|\boldsymbol{\Phi}\|_{H^1(\mathbb{R}^3)} \le C \, \|\mathbf{curl}\,\overline{\mathbf{u}}\|_{L^2(\mathbb{R}^3)} \,, \tag{5.5}$$

with $C = C(\Omega) > 0$. As a consequence

$$\mathbf{curl}(\overline{\mathbf{u}} - \boldsymbol{\Phi}) = 0 \quad \Rightarrow \quad \overline{\mathbf{u}} - \boldsymbol{\Phi} = \mathbf{grad} q \quad \text{in } \mathbb{R}^3 \,. \tag{5.6}$$

On every Ω_i, by definition $\overline{\mathbf{u}} = 0$, which implies $q_{|\Omega_i} \in H^2(\Omega_i)$. As the attached domains Ω_i are well separated Lipschitz domains, see Fig. 5.1, the H^2-extension of $q_{|\bigcup_i \Omega_i}$ to $\overline{q} \in H^2(\mathbb{R}^3)$ is possible. Moreover, it satisfies

$$\|\overline{q}\|_{H^2(\mathbb{R}^3)} \le C \|q\|_{H^2(\bigcup_i \Omega_i)} \le C \|\boldsymbol{\Phi}\|_{H^1(\mathbb{R}^3)} \le \|\mathbf{curl}\,\mathbf{u}\|_{L^2(\Omega)} \,. \tag{5.7}$$

$$\overline{\mathbf{u}} = \boldsymbol{\Phi} - \mathbf{grad}\overline{q} + \mathbf{grad}(q + \overline{q}) \,. \tag{5.8}$$

Finally, set $\boldsymbol{\Psi} := (\boldsymbol{\Phi} - \mathbf{grad}\overline{q})_{|\Omega}$, $p := q + \overline{q}$, and observe

$$\|\boldsymbol{\Psi}\|_{H^1(\Omega)} \le \|\boldsymbol{\Phi}\|_{H^1(\mathbb{R}^3)} + \|\overline{q}\|_{H^2(\mathbb{R}^3)} \le C \, \|\mathbf{curl}\,\mathbf{u}\|_{L^2(\Omega)} \,. \tag{5.9}$$

The constants may depend on Ω, Γ_D, and the chosen Ω_i. □

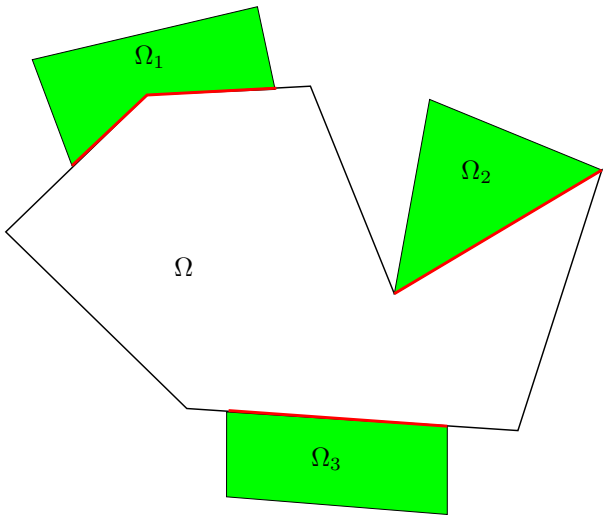

Fig. 5.1. Buffer zones attached to connected components of (red) Dirichlet boundary part Γ_D

The stable Helmholtz-type decomposition (5.2) immediately suggests the following idea: when given $\mathbf{v}_h \in \mathbf{U}(\mathcal{M}_h)$, first split it according to (5.2) and then attack both components by the uniformly H^1-stable local multilevel decompositions explored in the previous section. Alas, the idea is flawed, because neither of the terms in (5.2) is guaranteed to be a finite element function, even if this holds for $\mathbf{v}_h$.

Fortunately, the idea can be mended by building a purely discrete counterpart of (5.2) as in [29, Lemma 5.1] (called there "discrete regular decomposition"). For the sake of completeness we elaborate the proof below.

Lemma 5.1. *For any $\mathbf{v}_h \in \mathbf{U}(\mathcal{M}_h)$, there is $\mathbf{\Psi}_h \in (V(\mathcal{M}_h))^3$, $p_h \in V(\mathcal{M}_h)$, and $\widetilde{\mathbf{v}}_h \in \mathbf{U}(\mathcal{M}_h)$ such that*

$$\mathbf{v}_h = \widetilde{\mathbf{v}}_h + \mathbf{\Pi}_h \mathbf{\Psi}_h + \nabla p_h \,, \tag{5.10}$$

$$\|p_h\|_{H^1(\Omega)} \leq C \, \|\mathbf{v}_h\|_{\boldsymbol{H}(\mathbf{curl},\Omega)} \,, \tag{5.11}$$

$$\left\|h^{-1}\widetilde{\mathbf{v}}_h\right\|_{L^2(\Omega)} + \|\mathbf{\Psi}_h\|_{H^1(\Omega)} \leq C \, \|\mathbf{curl}\, \mathbf{v}_h\|_{L^2(\Omega)} \,, \tag{5.12}$$

where the constant C depends only on Ω, Γ_D, and the shape regularity of $\mathcal{M}_h$.

Proof. (*cf.* [29, Lemma 5.1]) We fix a $\mathbf{v}_h \in \mathbf{U}(\mathcal{M}_h)$ and use the stable regular decomposition of Thm. 5.2 to split it according to

$$\mathbf{v}_h = \mathbf{\Psi} + \mathbf{grad} p \,, \quad \mathbf{\Psi} \in (H^1_{\Gamma_D}(\Omega))^3 \,, \quad p \in H^1_{\Gamma_D}(\Omega) \,. \tag{5.13}$$

We have already known that the functions $\mathbf{\Psi}$ and p satisfy

$$\|\mathbf{\Psi}\|_{H^1(\Omega)} \leq C \, \|\mathbf{curl}\, \mathbf{v}_h\|_{L^2(\Omega)} \,, \qquad \|\mathbf{grad} p\|_{L^2(\Omega)} \leq C \, \|\mathbf{v}_h\|_{\boldsymbol{H}(\mathbf{curl},\Omega)} \,, \tag{5.14}$$

with constants depending only on Ω and Γ_D.

Next, note that in (5.13) $\mathbf{curl}\, \mathbf{\Psi} = \mathbf{curl}\, \mathbf{v}_h \in \mathbf{curl}\, \mathbf{U}(\mathcal{M}_h)$, and, owing to Lemma 2.1, $\mathbf{\Pi}_h \mathbf{\Psi}$ is well defined. Further, a commuting diagram property together with Lemma 2.3 implies

$$\mathbf{curl}(Id - \mathbf{\Pi}_h)\mathbf{\Psi} = 0 \quad \Rightarrow \quad \exists q \in H^1_{\Gamma_D}(\Omega) : \quad (Id - \mathbf{\Pi}_h)\mathbf{\Psi} = \mathbf{grad} q \,. \tag{5.15}$$

The estimate of Lemma 2.1 together with (5.14) yields

$$\left\|h^{-1}\mathbf{grad} q\right\|_{L^2(\Omega)} = \left\|h^{-1}(Id - \mathbf{\Pi}_h)\mathbf{\Psi}\right\|_{L^2(\Omega)} \leq C|\mathbf{\Psi}|_{H^1(\Omega)} \leq C \, \|\mathbf{curl}\, \mathbf{v}_h\|_{L^2(\Omega)} \,. \tag{5.16}$$

In order to push $\mathbf{\Psi}$ into a finite element space, a quasi-interpolation operator $\mathsf{Q}_h : (L^2(\Omega))^3 \mapsto (V(\mathcal{M}_h))^3$ is the right tool. We simply get it from componentwise application of a standard quasi-interpolation operator for linear Lagrangian finite elements, see [39, Sect. 2.1.1] and [43]. Thus, we can define the terms in the decomposition (5.10) as

$$\widetilde{\mathbf{v}}_h := \mathbf{\Pi}_h(\mathbf{\Psi} - \mathsf{Q}_h \mathbf{\Psi}) \in \mathbf{U}(\mathcal{M}_h) \,, \tag{5.17}$$

$$\mathbf{\Psi}_h := \mathsf{Q}_h \mathbf{\Psi} \in (V(\mathcal{M}_h))^3 \,, \tag{5.18}$$

$$\mathbf{grad} p_h := \mathbf{grad}(p + q) \,, \quad p_h \in V(\mathcal{M}_h) \,. \tag{5.19}$$

Indeed, $\mathbf{grad}(p + q) \in \mathbf{U}(\mathcal{M}_h)$ such that $p + q \in V(\mathcal{M}_h)$. The stability of the decomposition (5.10) can be established as follows: first, make use of Lemma 2.1, quasi-interpolation error

estimates, and the $H^1(\Omega)$-stability of quasi-interpolation to obtain, with $C = C(\rho_{\mathcal{M}_h}) > 0$,

$$\begin{aligned}\left\|h^{-1}\widetilde{\mathbf{v}}_h\right\|_{L^2(\Omega)} &\leq \left\|h^{-1}(Id - \mathbf{\Pi}_h)(\mathbf{\Psi} - \mathsf{Q}_h\mathbf{\Psi})\right\|_{L^2(\Omega)} + \left\|h^{-1}(Id - \mathsf{Q}_h)\mathbf{\Psi}\right\|_{L^2(\Omega)} \\ &\leq C|(Id - \mathsf{Q}_h)\mathbf{\Psi}|_{H^1(\Omega)} + |\mathbf{\Psi}|_{H^1(\Omega)} \\ &\leq C|\mathbf{\Psi}|_{H^1(\Omega)} \leq C\left\|\mathbf{curl}\,\mathbf{v}_h\right\|_{L^2(\Omega)} .\end{aligned}$$

Due to the definition (5.18), the next estimate is a simple consequence of the $H^1(\Omega)$-continuity of Q_h and Thm. 5.2

$$\|\mathbf{\Psi}_h\|_{H^1(\Omega)} \leq C\|\mathbf{\Psi}\|_{H^1(\Omega)} \leq C\left\|\mathbf{curl}\,\mathbf{v}_h\right\|_{L^2(\Omega)} . \tag{5.20}$$

Finally, the estimates established so far plus the triangle inequality yield

$$\|\mathbf{grad} p_h\|_{L^2(\Omega)} \leq C\left\|\mathbf{v}_h\right\|_{\boldsymbol{H}(\mathbf{curl},\Omega)} . \tag{5.21}$$

5.2. Local multilevel splitting of $\mathbf{U}(\mathcal{M}_h)$

With the discrete Helmholz-type decomposition of Lemma 5.1 at our disposal, we can now tackle its piecewise linear and continuous components with Thm. 5.1.

Lemma 5.2. *For any $\mathbf{v}_h \in \mathbf{U}(\mathcal{M}_h)$, there exists a constant C only depending on the domain, the Dirichlet boundary part Γ_D, the shape regularity of the meshes $\mathcal{M}_l$, $\widehat{\mathcal{M}}_l$, $0 \leq l \leq L$, and the constants in* (3.3)*, such that*

$$\mathbf{v}_h = \sum_{l=0}^{L}\Big(\mathbf{v}_l + \nabla p_l\Big), \quad \mathbf{v}_l \in \mathrm{Span}\left\{\mathfrak{B}_{\mathbf{U}}^l\right\},\ p_l \in \mathrm{Span}\left\{\mathfrak{B}_V^l\right\} , \tag{5.22}$$

and

$$\begin{aligned}&\|\mathbf{v}_0\|^2_{\boldsymbol{H}(\mathbf{curl},\Omega)} + |p_0|^2_{H^1(\Omega)} + \sum_{l=1}^{L} h_l^{-2}\left(\|\mathbf{v}_l\|^2_{L^2(\Omega)} + \|p_l\|^2_{L^2(\Omega)}\right) \\ &\leq C\left\|\mathbf{v}_h\right\|^2_{\boldsymbol{H}(\mathbf{curl},\Omega)} ,\end{aligned} \tag{5.23}$$

where $\mathfrak{B}_V^l$ and $\mathfrak{B}_{\mathbf{U}}^l$ are defined in (4.9)*.*

Proof. We start from the discrete Helmholtz-type decomposition of $\mathbf{v}_h$ in (5.10):

$$\mathbf{v}_h = \widetilde{\mathbf{v}}_h + \mathbf{\Pi}_h\mathbf{\Psi}_h + \nabla p_h, \quad \mathbf{\Psi}_h \in (V(\mathcal{M}_h))^3,\ p_h \in V(\mathcal{M}_h),\ \widetilde{\mathbf{v}}_h \in \mathbf{U}(\mathcal{M}_h).$$

We apply the result of Thm. 5.1 about the existence of stable local multilevel splittings of $V(\mathcal{M}_h)$ componentwise to $\mathbf{\Psi}_h$: this gives

$$\mathbf{\Psi}_h = \sum_{l=0}^{L}\mathbf{\Psi}_l , \quad \mathbf{\Psi}_l \in \mathrm{Span}\left\{\mathfrak{B}_V^l\right\}^3 , \tag{5.24}$$

$$|\mathbf{\Psi}_0|^2_{H^1(\Omega)} + \sum_{l=1}^{L} h_l^{-2}\left\|\mathbf{\Psi}_l\right\|^2_{L^2(\Omega)} \leq C|\mathbf{\Psi}_h|^2_{H^1(\Omega)} . \tag{5.25}$$

Observe that the functions $\boldsymbol{\Psi}_l$ do not belong to $\mathbf{U}(\mathcal{M}_l)$. Thus, we target them with edge element interpolation operators $\boldsymbol{\Pi}_l$ onto $\mathbf{U}(\mathcal{M}_l)$, see (2.7), and obtain the splitting described in Lemma 2.2:

$$\boldsymbol{\Psi}_l = \boldsymbol{\Pi}_l \boldsymbol{\Psi}_l + \nabla w_l \;, \quad w_l \in \widetilde{V}_2(\mathcal{M}_l) \;. \tag{5.26}$$

The gradient terms introduced by (5.26) are well under control: writing $s_h := \sum_{l=0}^{L} w_l$, the L^2-stability of (5.26), see Lemma 2.2, yields

$$\begin{aligned}
&\|\boldsymbol{\Pi}_l \boldsymbol{\Psi}_l\|_{L^2(\Omega)} \leq C \, \|\boldsymbol{\Psi}_l\|_{L^2(\Omega)} \;, \\
&|s_h|^2_{H^1(\Omega)} \leq C \Big(\sum_{l=0}^{L} \|\boldsymbol{\Psi}_l\|_{L^2(\Omega)} \Big)^2 \\
&\leq C \sum_{l=0}^{L} h_l^2 \cdot \sum_{l=0}^{L} h_l^{-2} \, \|\boldsymbol{\Psi}_l\|^2_{L^2(\Omega)} \overset{(5.25)}{\leq} C |\boldsymbol{\Psi}_h|^2_{H^1(\Omega)} \;.
\end{aligned}$$

Because of $\mathbf{curl}\, \boldsymbol{\Pi}_0 \boldsymbol{\Psi}_0 = \mathbf{curl}\, \boldsymbol{\Psi}_0$, we infer from (5.25)

$$\|\boldsymbol{\Pi}_0 \boldsymbol{\Psi}_0\|^2_{\boldsymbol{H}(\mathbf{curl},\Omega)} + \sum_{l=1}^{L} h_l^{-2} \, \|\boldsymbol{\Pi}_l \boldsymbol{\Psi}_l\|^2_{L^2(\Omega)} \leq C |\boldsymbol{\Psi}_h|^2_{H^1(\Omega)} \;. \tag{5.27}$$

Above and throughout the remainder of the proof, constants are independent of L.

By the projector property $\boldsymbol{\Pi}_h \circ \boldsymbol{\Pi}_l = \boldsymbol{\Pi}_l$, $l = 0, \ldots, L$, and the commuting diagram property (2.11), we arrive at

$$\mathbf{v}_h = \widetilde{\mathbf{v}}_h + \sum_{l=0}^{L} \boldsymbol{\Pi}_l \boldsymbol{\Psi}_l + \mathbf{grad}(\mathcal{I}_h s_h + p_h) \;, \tag{5.28}$$

where $\mathcal{I}_h$ is the nodal linear interpolation operator onto $V(\mathcal{M}_h)$. Recall (2.22) to see that

$$|\mathcal{I}_h s_h + p_h|_{H^1(\Omega)} \leq C |s_h|_{H^1(\Omega)} + |p_h|_{H^1(\Omega)} \leq C \, \|\mathbf{v}_h\|_{\boldsymbol{H}(\mathbf{curl},\Omega)} \;.$$

The local multilevel splitting of $\mathcal{I}_h s_h + p_h$ according to Thm. 5.1 gives

$$\mathcal{I}_h s_h + p_h = \sum_{l=0}^{L} p_l \;, \quad p_l \in \operatorname{Span}\big\{ \mathfrak{B}_V^l \big\} \;, \tag{5.29}$$

$$|p_0|^2_{H^1(\Omega)} + \sum_{l=1}^{L} h_l^{-2} \, \|p_l\|^2_{L^2(\Omega)} \leq C |\mathcal{I}_h s_h + p_h|^2_{H^1(\Omega)} \leq C \, \|\mathbf{v}_h\|^2_{\boldsymbol{H}(\mathbf{curl},\Omega)} \;. \tag{5.30}$$

Still, the contribution $\widetilde{\mathbf{v}}_h$ does not yet match (4.11). The idea is to distribute $\widetilde{\mathbf{v}}_h$ to the terms $\boldsymbol{\Pi}_l \boldsymbol{\Psi}_l$ by scale separation. To that end, we assign a level to each active edge of $\mathcal{M}_h$

$$\ell(E) := \min\{\ell(K) : \; K \in \mathcal{M}_h, \; E \text{ is edge of } K\} \;, \quad E \in \mathcal{E}(\mathcal{M}_h) \;. \tag{5.31}$$

Thus, we distinguish parts of $\widetilde{\mathbf{v}}_h$ on different levels: given the basis representation

$$\widetilde{\mathbf{v}}_h = \sum_{E \in \mathcal{E}(\mathcal{M}_h)} \alpha_E \mathbf{b}_E \;, \quad \{\mathbf{b}_E\}_{E \in \mathcal{E}(\mathcal{M}_h)} = \mathfrak{B}_{\mathbf{U}}(\mathcal{M}_h) \;, \tag{5.32}$$

we split

$$\widetilde{\mathbf{v}}_h = \sum_{l=0}^{L} \widetilde{\mathbf{v}}_l \ , \quad \widetilde{\mathbf{v}}_l := \sum_{\substack{E\in\mathcal{E}(\mathcal{M}_h)\\ \ell(E)=l}} \alpha_E \mathbf{b}_E \ , \quad \operatorname{supp}(\widetilde{\mathbf{v}}_l) \subset \overline{\omega}_l \ . \tag{5.33}$$

The estimate

$$\left\| h^{-1} \widetilde{\mathbf{v}}_h \right\|_{L^2(\Omega)} \leq C \left\| \mathbf{curl}\, \mathbf{v}_h \right\|_{L^2(\Omega)}$$

from Lemma 5.1 means that $\widetilde{\mathbf{v}}_h$ is "small on fine scales". Thanks to the L^2-stability (2.6) of the edge bases, this carries over to $\widetilde{\mathbf{v}}_l$:

$$\begin{aligned} \sum_{l=0}^{L} h_l^{-2} \left\| \widetilde{\mathbf{v}}_l \right\|^2_{L^2(\Omega)} &\leq C \sum_{l=0}^{L} h_l^{-2} \sum_{E\in\mathcal{E}(\mathcal{M}_h),\ell(E)=l} \alpha_E^2 \left\| \mathbf{b}_E \right\|^2_{L^2(\Omega)} \\ &\leq C \sum_{l=0}^{L} h_l^{-2} \sum_{E\in\mathcal{E}(\mathcal{M}_h),\ell(E)=l} \alpha_E^2 \left\| \mathbf{b}_E \right\|^2_{L^2(T_E)} \\ &\leq C \sum_{l=0}^{L} h_l^{-2} \left\| \widetilde{\mathbf{v}}_h \right\|^2_{L^2(\Sigma_l)} \leq C \left\| h^{-1} \widetilde{\mathbf{v}}_h \right\|^2_{L^2(\Omega)} \ , \end{aligned} \tag{5.34}$$

where $T_E \in \mathcal{M}_h$ is coarsest element adjacent to E, *cf.* (5.31), and refinement strips are defined by

$$\Sigma_l := \omega_l \setminus \overline{\omega_{l+1}} \ , \ 0 \leq l < L, \quad \Sigma_L := \omega_L \ , \tag{5.35}$$

see Figs. 4.1 and 4.2.

Yet, in the case of bisection refinement, $\widetilde{\mathbf{v}}_l$ may not be spanned by basis functions in $\mathfrak{B}^l_{\mathbf{U}}$, because the basis functions of $\mathbf{U}(\mathcal{M}_h)$ attached to each edge on $\overline{\Sigma_l} \bigcap \overline{\omega_{l+1}}$, $0 \leq l < L$ do not belong to any $\mathfrak{B}^l_{\mathbf{U}}$!

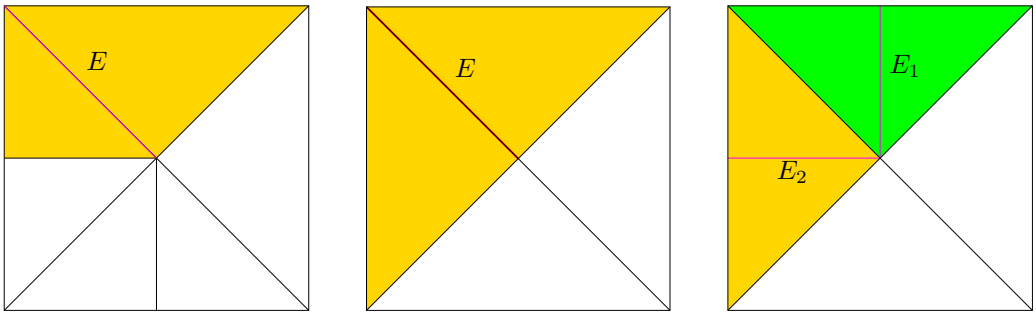

Edge E, support of basis function $\mathbf{b}_E$ | Support of $\mathbf{b}^l_E$ | Edges supporting $\mathbf{b}^{l+1}_{E_1}$, $\mathbf{b}^{l+1}_{E_2}$

Fig. 5.2. Basis function with which $\mathbf{b}_E$ can be represented

Take any $E \subset \overline{\Sigma_l} \bigcap \overline{\omega_{l+1}}$. Let $\mathbf{b}_E$, $\mathbf{b}^l_E$, and $\mathbf{b}^{l+1}_E$ be the basis functions of $\mathbf{U}(\mathcal{M}_h)$, $\mathbf{U}(\mathcal{M}_l)$, and $\mathbf{U}(\mathcal{M}_{l+1})$ associated with E, see Fig. 5.2 for a 2D illustration. Denote by $K_1, \ldots, K_n$ all elements in ω_{l+1} and $\mathcal{M}_l$ which contain E, and by $E_1, \ldots, E_m$ their new edges connecting E but

not contained in the refinement edges of $K_1, \ldots, K_n$ (see Fig. 5.3). Supposing the orientations of each E_i and E point to their common endpoint, we have

$$\mathbf{b}_E = \mathbf{b}_E^l + \frac{1}{2}\sum_{i=1}^{m} \mathbf{b}_{E_i}^{l+1} \,. \tag{5.36}$$

This decomposition is L^2-stable with constants merely depending on shape regularity.

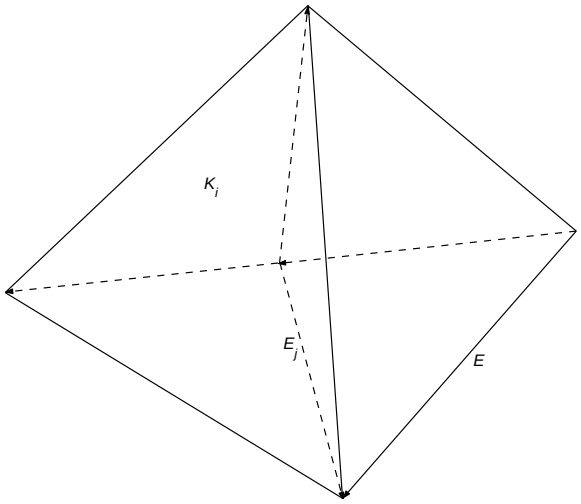

Fig. 5.3. Situation at an edge E lying on the interface between Σ_l and ω_{l+1}.

Since $\sum_{i=1}^{m} \mathbf{b}_{E_i}^{l+1} \in \mathfrak{B}_{\mathbf{U}}^{l+1}$, we may move the component of $\widetilde{\mathbf{v}}_l$ associated with this term to $\widetilde{\mathbf{v}}_{l+1}$ for any E. Then the decomposition (5.33) and the stability estimate (5.34) remain valid.

Summing up, the stability estimate (5.27) is preserved after replacing $\mathbf{\Pi}_l \mathbf{\Psi}_h$ with $\mathbf{\Pi}_l \mathbf{\Psi}_h + \widetilde{\mathbf{v}}_l \in \mathbf{U}(\mathcal{M}_l)$. □

Eventually, the proof of Thm. 4.2 is readily accomplished. With Lemma 5.2 at our disposal, we merely appeal to the L^2-stabilities expressed in (2.6) and (2.9) and inverse inequalities to see that all components in (5.22) can be split into local contributions of basis functions in $\mathfrak{B}_{\mathbf{U}}^l$ and $\mathfrak{B}_V^l$, respectively.

6. Numerical Experiments

In the reported numerical experiments the implementation of adaptive mesh refinement was based on the adaptive finite element package ALBERTA [41], which uses the bisection strategy of [33], see Sect. 3.

Let $\mathcal{M}_0$ be an initial mesh satisfying the two assumptions (A1) and (A2) in [33, P. 282], the adaptive mesh refinements are governed by a residual based a posteriori error estimator. In the experiments we assume the current density $\mathbf{f} \in \boldsymbol{H}(\mathrm{div}, \Omega)$ and use the estimator given by [17, §5]: given a finite element approximation $\mathbf{u}_h \in \mathbf{U}(\mathcal{M}_h)$, for any $T \in \mathcal{M}_h$

$$\eta_T^2 := h_T^2 \|\mathbf{f} - \mathbf{u}_h\|_{\boldsymbol{H}(\mathrm{div},T)}^2 + \frac{h_T}{2} \sum_{F \subset \partial T} \Big\{ \|[\mathbf{u}_h]_F\|_{0,F}^2 + \|[\mathbf{curl}\, \mathbf{u}_h \times \boldsymbol{\nu}]_F\|_{0,F}^2 \Big\},$$

where F is a face of T, $\boldsymbol{\nu}$ is the unit normal of F, and $[\mathbf{u}_h]_F$ is the jump of $\mathbf{u}_h$ across F. The global a posteriori error estimate and the maximal estimated element error on $\mathcal{M}_h$ are defined by

$$\eta_h := \left(\sum_{T \in \mathcal{M}_h} \eta_T^2 \right)^{1/2}, \qquad \eta_{\max} = \max_{T \in \mathcal{M}_h} \eta_T. \tag{6.1}$$

Using η_h and $\eta_{\max}$, we use [17, Algorithm 5.1] to mark and refine $\mathcal{M}_h$ adaptively.

In the following, we report two numerical experiments to demonstrate the competitive behavior of the local multigrid method and to validate our convergence theory.

Example 6.1. *We consider the Maxwell equation on the three-dimensional "L-shaped" domain* $\Omega = (-1,\ 1)^3 \backslash \{(0,\ 1) \times (-1,\ 0) \times (-1,\ 1)\}$. *The Dirichlet boundary condition and the righthand side* $\mathbf{f}$ *are chosen so that the exact solution is*

$$\mathbf{u} := \nabla \left\{ r^{1/2} \sin(\phi/2) \right\}$$

in cylindrical coordinates (r, ϕ, z).

Table 6.1 shows the numbers of multigrid iterations required to reduce the initial residual by a factor 10^{-8} on different levels. We observe that the multigrid algorithm converges in almost the same small number of steps, though the number of elements varies from 156 to 100,420.

Table 6.1: The number of adaptive iterations $N_{\rm it}$, the number of elements $N_{\rm el}$, the number of multigrid iterations N_{itrs} required to reduce the initial residual by a factor 10^{-8}, the relative error between the true solution $\mathbf{u}$ and the discrete solution $\mathbf{u}_h$: $E_{\rm rel} = \|\mathbf{u} - \mathbf{u}_h\|_{\mathbf{H}(\mathbf{curl},\Omega)} \,/\, \|\mathbf{u}\|_{\mathbf{H}(\mathbf{curl},\Omega)}$ (Example 6.1).

$N_{\rm it}$	2	5	10	15	20	25	30	35
$N_{\rm el}$	156	388	1,900	4,356	9608	19,424	48,088	100,420
$E_{\rm rel}$	0.4510	0.3437	0.2456	0.1919	0.1600	0.1350	0.1094	0.0915
N_{itrs}	11	21	19	19	19	19	19	19

Fig. 6.1 (left) plots the CPU time versus the number of degrees of freedom on different adaptive meshes. It shows that the CPU time of solving the algebraic system increases roughly linearly with respect to the number of elements. Fig. 6.1 (rught) depicts a locally refined mesh of 100,420 elements created by the adaptive finite element algorithm.

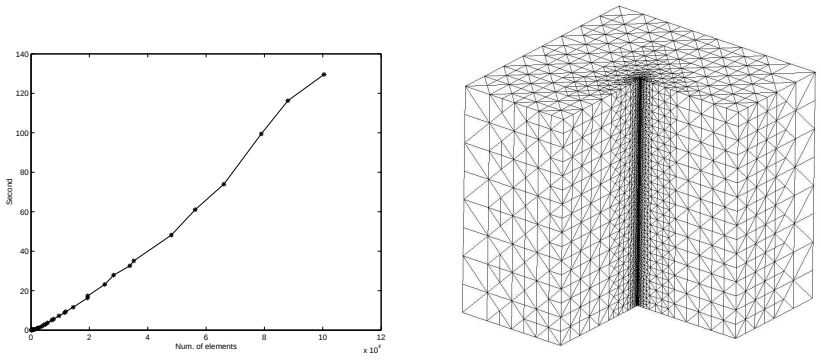

Fig. 6.1. Example 6.1, left: execution time for local multigrid method, right: instance of a locally refined mesh (100,420 elements)

Table 6.2: The number of adaptive iterations $N_{\rm it}$, the number of elements $N_{\rm el}$, the number of multigrid iterations N_{itrs} required to reduce the initial residual by a factor 10^{-8}, the relative error between the true solution $\mathbf{u}$ and the discrete solution $\mathbf{u}_h$: $E_{\rm rel} = \|\mathbf{u}-\mathbf{u}_h\|_{\mathbf{H(curl},\Omega)} / \|\mathbf{u}\|_{\mathbf{H(curl},\Omega)}$ (Example 6.2).

$N_{\rm it}$	2	5	10	15	20	25	30	33
$N_{\rm el}$	128	404	1,236	3,416	12,420	29,428	81,508	135,876
$E_{\rm rel}$	0.4616	0.3762	0.2992	0.2347	0.1752	0.1394	0.1095	0.0958
N_{itrs}	14	30	25	26	26	27	27	27

Example 6.2. *This example uses the same solution as Example* 6.1

$$\mathbf{u} := \nabla \left\{ r^{1/2} \sin(\phi/2) \right\}$$

in cylindrical coordinates (r, ϕ, z). *But the computational domain is changed to a three-dimensional non-Lipschitz domain with an inner crack-type boundary, which is defined by*

$$\Omega = (-1,\ 1)^3 \setminus \{(x, 0, z) :\ 0 \le x < 1,\ -1 < z < 1\}.$$

The Dirichlet boundary condition and the source function $\mathbf{f}$ *are the same as above.*

Table 6.2 records the numbers of multigrid iterations required to reduce the initial residual by a factor 10^{-8} on different levels. We observe that the multigrid algorithm converges in less than 30 steps, with the number of elements soaring from 128 to 135,876.

Fig. 6.2 (left) shows the CPU time versus the number of degrees of freedom on different adaptive meshes. Obviously, the CPU time for solving the algebraic system increases nearly linearly with respect to the number of elements.

Fig. 6.2 (right) displays a locally refined mesh of 135,876 elements using adaptive finite element algorithm. In addition, the restriction of the mesh to the cross-section $\{y = 0\}$, which contains the inner boundary, is drawn. This reveals strong local refinement.

This experiment bears out that the local multigrid is also efficient for the problems in non-Lipschitz doamins, which are outside the scope of our theory.

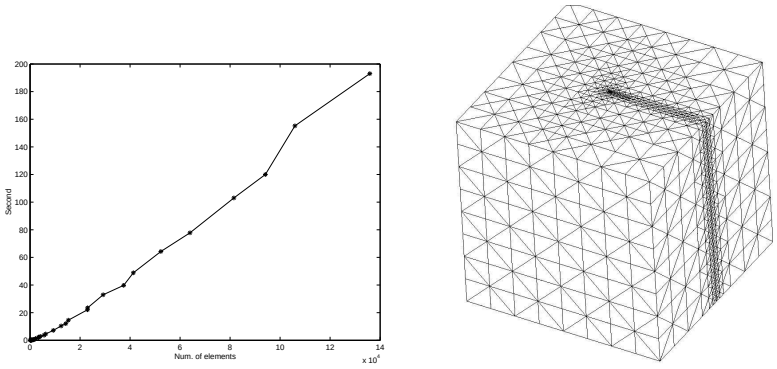

Fig. 6.2. Example 6.2, left: CPU time for solving the algebraic system by multigrid method, right: a locally refined mesh (135,876 elements)

Acknowledgements. The authors would like to thank Dr. L. Wang of Computer Network Information Center, Prof. Z. Chen and Prof. L. Zhang of the Institute of Computational Mathematics, Chinese Academy of Sciences, for their support in the implementation of the local

multigrid method. They are grateful to one referees who detected an error in an earlier version of the manuscript. The second author was supported in part by China NSF under the grant 60873177 and by the National Basic Research Project under the grant 2005CB321702.

References

[1] M. Ainsworth and W. McLean, Multilevel diagonal scaling preconditioners for boundary element equations on locally refined meshes, *Numer. Math.*, **93** (2003), 387-413.

[2] D. Arnold, R. Falk, and R. Winther, Multigrid in $H(\mathrm{div})$ and $H(\mathbf{curl})$, *Numer. Math.*, **85** (2000), 175-195.

[3] ———, Finite element exterior calculus, homological techniques, and applications, *Acta Numerica*, **15** (2006), 1-155.

[4] D. Arnold, A. Mukherjee, and L. Pouly, Locally adapted tetrahedral meshes using bisection, *SIAM J. Sci. Comput.*, **22** (2000), 431-448.

[5] D. Bai and A. Brandt, Local mesh refinement multilevel techniques, *SIAM J. Sci. Comput.*, **8** (1987), 109-134.

[6] E. Bänsch, Local mesh refinement in 2 and 3 dimensions, IMPACT *Comput. Sci. Eng.*, **3** (1991), 181-191.

[7] R. Beck, P. Deuflhard, R. Hiptmair, R. Hoppe, and B. Wohlmuth, Adaptive multilevel methods for edge element discretizations of Maxwell's equations, *Surveys on Mathematics for Industry*, **8** (1998), 271-312.

[8] R. Beck, R. Hiptmair, R. Hoppe, and B. Wohlmuth, Residual based a-posteriori error estimators for eddy current computation, $\mathrm{M}^2\mathrm{AN}$, **34** (2000), 159-182.

[9] J. Bey, Tetrahedral grid refinement, *Computing*, **55** (1995), 355-378.

[10] P. Binev, W. Dahmen, and R. DeVore, Adaptive finite element methods with convergence rates, *Numer. Math.*, **97** (2004), 219-268.

[11] F. Bornemann and H. Yserentant, A basic norm equivalence for the theory of multilevel methods, *Numer. Math.*, **64** (1993), 455-476.

[12] A. Bossavit, Whitney forms: A class of finite elements for three-dimensional computations in electromagnetism, *IEE Proc. A*, **135** (1988), 493-500.

[13] ———, Computational Electromagnetism. Variational Formulation, Complementarity, Edge Elements, vol. 2 of Electromagnetism Series, Academic Press, San Diego, CA, 1998.

[14] J. Bramble and J. Pasciak, New estimates for multilevel methods including the V-cycle, *Math. Comput.*, **60** (1993), 447-471.

[15] J. Bramble, J. Pasciak, J. Wang, and J. Xu, Convergence estimates for product iterative methods with applications to domain decomposition, *Math. Comput.*, **57** (1991), 1-21.

[16] A. Buffa, M. Costabel, and D. Sheen, On traces for $\mathbf{H}(\mathbf{curl}, \Omega)$ in Lipschitz domains, *J. Math. Anal. Appl.*, **276** (2002), 845-867.

[17] Z.-M. Chen, L. Wang, and W.-Y. Zheng, An adaptive multilevel method for time-harmonic Maxwell equations with singularities, *SIAM J. Sci. Comput.*, **29** (2008), 118-138.

[18] P. Ciarlet, The Finite Element Method for Elliptic Problems, vol. 4 of Studies in Mathematics and its Applications, North-Holland, Amsterdam, 1978.

[19] M. Clemens, S. Feigh, and T. Weiland, Geometric multigrid algorithms using the conformal finite integration technique, *IEEE T. Magn.*, **40** (2004), 1065-1068.

[20] M. Costabel and M. Dauge, Singularities of electromagnetic fields in polyhedral domains, *Arch. Ration. Mech. An.*, **151** (2000), 221-276.

[21] M. Costabel, M. Dauge, and S. Nicaise, Singularities of eddy current problems, *ESAIM: Math. Model. Num.*, **37** (2003), 807-831.

[22] V. Girault and P. Raviart, Finite Element Methods for Navier-Stokes Equations, Springer, Berlin, 1986.

[23] J. Gopalakrishnan, J. Pasciak, and L. Demkowicz, Analysis of a multigrid algorithm for time harmonic Maxwell equations, *SIAM J. Numer. Anal.*, **42** (2003), 90-108.
[24] V. Gradinaru and R. Hiptmair, Whitney elements on pyramids, *Electron. T. Numer. An.*, **8** (1999), 154-168.
[25] R. Hiptmair, Multigrid method for Maxwell's equations, *SIAM J. Numer. Anal.*, **36** (1999), 204-225.
[26] ———, Finite elements in computational electromagnetism, *Acta Numerica*, **11** (2002), 237-339.
[27] ———, Analysis of multilevel methods for eddy current problems, *Math. Comput.*, **72** (2003), 1281-1303.
[28] R. Hiptmair, G. Widmer, and J. Zou, Auxiliary space preconditioning in $\mathbf{H}_0(\mathbf{curl}, \Omega)$, *Numer. Math.*, **103** (2006), 435-459.
[29] R. Hiptmair and J. Xu, Nodal auxiliary space preconditioning in H(curl) and H(div) spaces, *SIAM J. Numer. Anal.*, **45** (2007), 2483-2509.
[30] R. Hiptmair and W.-Y. Zheng, Local multigrid in $\mathbf{H}(\mathbf{curl})$, Tech. Rep. 2007-03, SAM, ETH Zürich, Zürich, Switzerland, March 2007. `http://arxiv.org/abs/0901.0764.`
[31] R. Hoppe and J. Schöberl, Convergence of adaptive edge element methods for the 3D eddy currents equation, *J. Comput. Math.*, (2009). To appear.
[32] T. Kolev and P. Vassilevski, Parallel auxiliary space AMG for $\mathbf{H}(\mathbf{curl})$ problems, *J. Comput. Math.*, (2008).
[33] I. Kossaczký, A recursive approach to local mesh refinement in two and three dimensions, *J. Comput. Appl. Math.*, **55** (1994), 275-288.
[34] J. Maubach, Local bisection refinement for n–simplicial grids generated by reflection, *SIAM J. Sci. Comput.*, **16** (1995), 210-227.
[35] W. Mitchell, A comparison of adaptive refinement techniques for elliptic problems, *ACM T. Math. Software*, **15** (1989), 326-347.
[36] ———, Optimal multilevel iterative methods for adaptive grids, *SIAM J. Sci. Comput*, **13** (1992), 146-167.
[37] P. Monk, Finite Element Methods for Maxwell's Equations, Clarendon Press, Oxford, UK, 2003.
[38] J. Nédélec, Mixed finite elements in $\mathbb{R}^3$, *Numer. Math.*, **35** (1980), 315-341.
[39] P. Oswald, Multilevel Finite Element Approximation, Teubner Skripten zur Numerik, B.G. Teubner, Stuttgart, 1994.
[40] J. Pasciak and J. Zhao, Overlapping Schwarz methods in H(curl) on polyhedral domains, *J. Numer. Math.*, **10** (2002), 221-234.
[41] A. Schmidt and K. Siebert, ALBERTA – An adaptive hierarchical finite element toolbox. Website. ALBERTA is available online from `http://www.alberta-fem.de`.
[42] A. Schmidt and K. Siebert, Design of Adaptive Finite Element Software: The Finite Element Toolbox ALBERTA, Lecture Notes in Computational Science and Engineering, Springer, Heidelberg, 2005.
[43] J. Schöberl, Commuting quasi-interpolation operators for mixed finite elements, Preprint ISC-01-10-MATH, Texas A&M University, College Station, TX, 2001.
[44] ———, A multilevel decomposition result in $H(curl)$, in Proceedings of the 8th European Multigrid Conference 2005, Scheveningen, P. H. P. Wesseling, C.W. Oosterlee, ed., 2006.
[45] ———, A posteriori error estimates for Maxwell equations, *Math. Comput.*, **77** (2008), 633-649.
[46] O. Sterz, A. Hauser, and G. Wittum, Adaptive local multigrid methods for solving time-harmonic eddy current problems, *IEEE T. Magn.*, **42** (2006), 309-318.
[47] R. Stevenson, Optimality of a standard adaptive finite element method, *Found. Comput. Math.*, **7** (2007), 245-269.
[48] ———, The completion of locally refined simplicial partitions created by bisection, *Math. Comput.*, **77** (2008), 227-241.
[49] C. Traxler, An algorithm for adaptive mesh refinement in n dimensions, *Computing*, **59** (1997),

115-137.

[50] B. Weiss and O. Biro, Multigrid for time-harmonic 3-d eddy-current analysis with edge elements, *IEEE T. Magn.*, **41** (2005), 1712-1715.

[51] H. Whitney, Geometric Integration Theory, Princeton University Press, Princeton, 1957.

[52] H.-J. Wu and Z.-M. Chen, Uniform convergence of multigrid V-cycle on adaptively refined finite element meshes for second order elliptic problems, *Sci. China: Ser. A.*, **49** (2006), 1C28.

[53] J. Xu, Iterative methods by space decomposition and subspace correction, *SIAM Rev.*, **34** (1992), 581-613.

[54] ———, An introduction to multilevel methods, in Wavelets, Multilevel Methods and Elliptic PDEs, M. Ainsworth, K. Levesley, M. Marletta, and W. Light, eds., Numerical Mathematics and Scientific Computation, Clarendon Press, Oxford, 1997, 213-301.

[55] J. Xu and Y.-R. Zhu, Uniformly convergent multigrid methods for elliptic problems with strongly discontinuous coefficients, *Math. Mod. Meth. Appl. S.*, **18** (2008), 77-105.

[56] J. Xu and L. Zikatanov, The method of alternating projections and the method of subspace corrections in Hilbert space, *J. Am. Math. Soc.*, **15** (2002), 573-597.

[57] H. Yserentant, Old and new convergence proofs for multigrid methods, *Acta Numerica*, (1993), 285-326.